High-precision measurements of $n = 2 \rightarrow n = 1$ transition energies and level widths in He- and Be-like Argon Ions

J. Machado, C. I. Szabo, J. P. Santos, P. Amaro, M. Guerra, A. Gumberidze, Guojie Bian, J. M. Isac, P. Indelicato

High-precision measurements of $n = 2 \rightarrow n = 1$ transition energies and level widths in He- and Be-like Argon Ions

J. Machado,[1,2] C. I. Szabo,[3] J. P. Santos,[1] P. Amaro,[1] M. Guerra,[1]
A. Gumberidze,[4] Guojie Bian,[2,5] J. M. Isac,[2] and P. Indelicato[2]

[1]*Laboratório de Instrumentação, Engenharia Biomédica e Física da Radiação (LIBPhys-UNL), Departamento de Física, Faculdade de Ciências e Tecnologia, FCT, Universidade Nova de Lisboa, 2829-516 Caparica, Portugal*

[2]*Laboratoire Kastler Brossel, UPMC-Sorbonne Universités, CNRS, ENS-PSL Research University, Collège de France, Case 74; 4, place Jussieu, F-75005 Paris, France*

[3]*Theiss Research, La Jolla, CA 92037, USA*

[4]*ExtreMe Matter Institute EMMI and Research Division, GSI Helmholtzzentrum fr Schwerionenforschung, D-64291 Darmstadt, Germany*

[5]*Institute of Atomic and Molecular Physics, Sichuan University, Chengdu 610065, P.R. China*

(Dated: July 25, 2017)

Abstract

We performed a reference-free measurement of the transition energies of the $1s2p\,^1P_1 \rightarrow 1s^2\,^1S_0$ line in He-like argon, and of the $1s2s^22p\,^1P_1 \rightarrow 1s^22s^2\,^1S_0$ line in Be-like argon ions. The highly-charged ions were produced in the plasma of an Electron-Cyclotron Resonance Ion Source. Both energy measurements were performed with an accuracy better than 3 parts in 10^6, using a double flat-crystal spectrometer, without reference to any theoretical or experimental energy. The $1s2s^22p\,^1P_1 \rightarrow 1s^22s^2\,^1S_0$ transition measurement is the first reference-free measurement for this core-excited transition. The $1s2p\,^1P_1 \rightarrow 1s^2\,^1S_0$ transition measurement confirms recent measurement performed at the Heidelberg Electron-Beam Ion Trap (EBIT). The width measurement in the He-like transition provides test of a purely radiative decay calculations. In the case of the Be-like argon transition, the width results from the sum of a radiative channel and three main Auger channels. We also performed Multiconfiguration Dirac-Fock (MCDF) calculations of transition energies and rates and have done an extensive comparison with theory and other experimental data. For both measurements reported here, we find agreement with the most recent theoretical calculations within the combined theoretical and experimental uncertainties.

PACS numbers: 34.80.Dp, 34.50.Fa, 34.10.+x

I. INTRODUCTION

Bound-states quantum electrodynamics (BSQED) and the relativistic many-body problem have been undergoing important progress in the past few years. Yet there are several issues that require increasing the number of high-precision tests. High-precision measurements of transition energies on medium to high-Z elements [1–9], Landé g-Factors [10–16], hyperfine structure[17–29], just to name a few, are needed either to improve our understanding or to provide tests of higher-order QED-corrections, the calculations of which are very demanding.

Recent measurement of the proton size in muonic hydrogen [30, 31] and of the deuteron in muonic deuterium [32], which disagree by 7 and 3.5 standard deviations respectively from measurements in their electronic counterparts triggered experimental and theoretical research regarding not only the specific issue of the proton and deuteron size, but also the possible anomalies in BSQED. A discrepancy of this magnitude, corresponds to a difference in the muonic hydrogen energy of 0.42 meV, which is far outside the calculations uncertainty of about ± 0.01 meV and is much larger than can be expected from any omitted QED contribution. An other large discrepancy of 7 standard deviations between theory and experiment has also been observed recently in a specific difference between the hyperfine structures of hydrogen-like and lithium-like bismuth measured at the ESR in Darmstadt [29], designed to eliminate the effect of the nuclear magnetization distribution (the Bohr-Weisskopf correction) [22].

Medium-Z, few-electron ions, with a K hole are the object of the present work. They have been studied first in laser-produced plasmas [33] and beam-foil spectroscopy [34, 35], or by using the interaction of fast ion beams with gas targets in heavy-ion accelerators. Ion storage rings have also been used [36–38]. The limitation in precision of those measurements is mostly due to the large Doppler effect, which affects energy measurements, and the Doppler broadening, which affects any possible width measurement. Recoil ion spectroscopy [39], which has also been used, is not affected. Plasma machines, like tokamaks have also provided spectra[40, 41], providing relative measurements, usually using He-like lines as a reference. Solar measurements [42] have also been reported.

Recently, accurate transition energy measurements in medium-Z highly-charged ions have been reported recently using either Electron Beam Ion Trap (EBIT) or Electron-Cyclotron

Ion Sources (ECRIS) to produce the ions. Measurements of transition energies in one and two-electron ions using an EBIT have been performed by the Livermore group [8], Heidelberg group [1, 4, 9, 43] and the Melbourne and NIST collaboration [3, 5, 6]. The present collaboration has reported values using an ECRIS [2].

The Heidelberg group reported the measurement of the $1s2p\,^1P_1 \rightarrow 1s^2\,^1S_0$ He-like argon line with a relative accuracy of 1.5×10^{-6} without the use of a reference line [43]. In that work, the spectrometer used is made of a single flat Bragg crystal coupled to a CCD camera, which can be positioned very accurately with a laser beam reflected by the same crystal as the x rays [43]. The Melbourne-NIST collaboration reported the measurement of all the $n = 2 \rightarrow n = 1$ transitions in He-like titanium with a relative accuracy of 15×10^{-6}, using a calibration based on neutral x-ray lines emitted from an electron fluorescence x-ray source [3, 5, 6]. The Livermore group reported a measurement of all $n = 2 \rightarrow n = 1$ lines in helium-like copper [8], using hydrogen-like lines in argon as calibration. It also reported measurement of all 4 lines in He-like xenon, using a micro-calorimeter and calibration with x-ray standards [44]. It should be emphasized that measurements in both type of ion sources do not require Doppler shift correction to transition energy measurements, because the ions have only thermal motion.

Measurements of the $1s2s^22p\,^1P_1 \rightarrow 1s^22s^2\,^1S_0$ line in Be-like ions are scarce. Some measurements are relative measurements using tokamaks, where the Be-like line appears as a satellite line for the He-like $2 \rightarrow 1$ transitions. The $1s2p\,^1P_1 \rightarrow 1s^2\,^1S_0$ line is often used as a calibration. Measurements of that type for Be-like Ar have been performed at TFR [45], and for Ni at TFTR [40, 41]. Such relative measurements, which use theoretical results on the He-like line, must be re-calibrated, using the most recent theoretical values. Several other observations have been made on different elements, but no experimental energy reported (see, e.g. Ref. [46] for Cl, Ar and Ca), or the experimental accuracy is not completely documented (see e.g., [47–49]). Measurements in EBIT are also known, as in vanadium [50] and iron [51], for terrestrial and astrophysics plasma applications. There have also been relative measurements in ECRIS for sulfur, chlorine and argon [52], using the relativistic M1 transition $1s2s\,^3S_1 \rightarrow 1s^2\,^1S_0$ as a reference.

Chantler *et al.* [3, 5, 53], have claimed that existing data show the evidence of a discrepancy between the most advanced BSQED calculation [54] and measurements in the He-like isoelectronic sequence, leading to a deviation that scales as $\approx Z^3$. They speculated [5]

that this supposed systematic effect could provide insight into the *proton size puzzle*, the Rydberg and fine-structure constants, or missing three-body BSQED terms. Here we make a detailed analysis, including all available experimental results, to check this claim.

We emphasize the advantage of studying highly-charged, medium-Z systems, such as argon ions, to test QED. The BSQED contributions have a strong Z-dependence: the retardation correction to the electron-electron interaction contribution scales as Z^3, and the one-electron corrections, self-energy and vacuum polarization, scale as Z^4. Yet, at high-Z, the strong enhancement of the nuclear size contribution and associated uncertainty limits the degree to which available experimental measurements can be used to test QED [53, 55–58]. At very low-Z, experiments can be much more accurate, but tests of QED can be limited as well, even for very accurate measurements of transitions to the ground state of He [59–61]. For few-electron atoms and ions, they are limited by the large size of electron-electron correlation and, by the evaluation of the needed higher-order QED screening corrections, in the non-relativistic QED formalism (NRQED) [62–66]. It can also be limited by the slow convergence of all-order QED contributions at low-Z, which may be required for comparison, and because of the insufficient knowledge of some nuclear parameters, namely the form factors and polarization [30–32, 54]. In medium-Z elements like argon or iron, the nuclear mean spherical radii are sufficiently well known (see, e.g., [67]) and nuclear polarization is very small. So uncertainties related to the nucleus are small compared to experimental and theoretical accuracy. This can be seen in the theoretical uncertainties claimed in Ref. [54].

Besides the fundamental aspect, knowledge of transition energies and wavelengths of highly-charged ions is very important for many sectors of research, like astrophysics or plasma physics. For example, an unidentified line was recently detected at 3.55 keV-3.57(3) keV in an XMM-Newton space x-ray telescope spectrum of 73 galaxy clusters[68] and at 3.52(3) keV for another XMM spectrum in the Andromeda galaxy and the Perseus galaxy cluster [69]. The next year a line at 3.539(11) keV was observed in the deep exposure data set of the Galactic center region with the same instrument. A possible connection with a dark matter decay line has been put forward, yet measurements performed with an EBIT seems to show that it could be a set of lines in highly charged sulfur ions, induced by charge exchange [70].

In the present work, we apply the method we have developed to measure the energy and line-width of the $1s2s\,^3S_1 \rightarrow 1s^2\,^1S_0$ M1 transition reported in Ref. [2], to the $1s2p\,^1P_1 \rightarrow$

$1s^2\,{}^1S_0$ transition in He-like argon and to the $1s^22s2p\,{}^1P_1 \rightarrow 1s^22s^2\,{}^1S_0$ transition in Be-like argon ions. We also present a multi-configuration Dirac-Fock (MCDF) calculation for the two transition energies and widths. These calculations are performed with a new version of the *mcdfgme* code that uses the effective operators developed by the St Petersburg group to evaluate the self-energy screening [71].

The article is organized as follows. In the next section we briefly describe the experimental setup used in this work. A detailed description of the analysis method that provides the energy, width and uncertainties is given in Sec. III. A brief description of the calculations of transition energy and widths is given in Sec. IV. We present our experimental result for the $1s2p\,{}^1P_1 \rightarrow 1s^2\,{}^1S_0$ in Sec. V. In the same section we present all available experimental results for $7 \leq Z \leq 92$ and $n = 2 \rightarrow n = 1$ transitions. We do a very detailed comparison between theory from Ref. [54], which covers $12 \leq Z \leq 92$ and the available measurements in this Z-range. Our results and comparison with theory for the $1s2s^22p\,{}^1P_1 \rightarrow 1s^22s^2\,{}^1S_0$ line in Be-like argon ions are presented in Sec. VI. The conclusions are provided in Sec. VII.

II. EXPERIMENTAL METHOD

ECRIS plasmas have been shown to be very intense sources of x rays, and have diameters of a few cm. Therefore, they are better adapted to spectrometers that can use an extended source. At low energies, cylindrically or spherically bent crystal spectrometers as well as double-crystal spectrometers (DCSs) can be used.

A single flat-crystal spectrometer, combined with an accurate positioning of the detector, and alternate measurements, symmetrical with respect to the optical axis of the instrument, as used in Heidelberg [43], and the double-crystal spectrometers [72, 73] are the only two methods that can provide high-accuracy, reference-free measurements in the x-ray domain. Our group reported in 2012 the measurement of the $1s2s\,{}^3S_1 \rightarrow 1s^2\,{}^1S_0$ transition energy in He-like argon with an uncertainty of 2.5×10^{-6} without the use of an external reference [2], using the same experimental device as in the present work: a DCS connected to an ECRIS, the "Source d' Ions Multichargés de Paris" (SIMPA)[74], jointly operated by the Laboratoire Kastler Brossel and the Institute des Nanosciences de Paris on the Université Pierre and Marie Curie campus.

A detailed description of the experimental setup of the DCS at the SIMPA ECRIS used

in this work is given in Ref. [73]. A neutral gas (Ar in the present study) is injected into the plasma chamber inside a magnetic system with minimum fields at the very center of the vacuum chamber. Microwaves at a frequency of 14.5 GHz heat the electrons that are trapped by the magnetic field. The energetic electrons ionize the gas through repeated collisions reaching up to helium-like charge states [75]. The ions are, in turn, trapped by the space charge of the electrons, which have a density around $1 \times 10^{11}\,\mathrm{cm}^{-3}$. This corresponds to a trapping potential of a fraction of 1 V, leading to an ion-speed distribution of ≈1 eV per charge, and thus to a small Doppler broadening of all the observed lines. In contrast, EBITs have a trapping potential of several hundred eV, and the Doppler broadening is then much larger.

The $1s2s\,^3S_1$ state is mostly created by electron ionization of the $1s^22s\,^2S_{1/2}$ ground state of Li-like argon, and therefore the $1s2s\,^3S_1 \rightarrow 1s^2\,^1S_0$ line is the most intense line we observed in He-like argon. The $1s2p\,^1P_1 \rightarrow 1s^2\,^1S_0$ line observed here results from the excitation of the $1s^2\,^1S_0$ He-like argon ground state, which is much less abundant, leading to a weaker line. The Be-like excited level, $1s2s^22p\,^1P_1$, is mostly produced by ionization of the ground state of boron-like argon, which is a well-populated charge-state (see Fig. 21, Ref. [73]). The $1s2s^22p\,^1P_1 \rightarrow 1s^22s^2\,^1S_0$ line is thus the most intense we observed.

The spectra are recorded by a specially-designed, reflection vacuum double-crystal spectrometer described in detail in Ref. [73]. The two $6 \times 4\,\mathrm{cm}^2$, 6 mm-thick Si(111) crystals were made at the National Institute for Standards and Technology (NIST). Their lattice spacing in vacuum was measured and found to be d =1.135 601 048(38) Å (relative uncertainty of 0.012×10^{-6}) at a temperature of 22.5 °C [73], relative to the standard value [76, 77]. More details will be found in Ref. [78]. Using this lattice spacing, our measurements provides wavelengths directly tied to the definition of the meter [77]. The DCS is connected to the ion source in such a way that the axis of the spectrometer is aligned with the ECRIS axis and is located at 1.2 m from the plasma (a sphere of ≈ 3 cm in diameter).

To analyse the experimental spectra, we developed a simulation code [73], which uses the geometry of the instrument and of the x-ray source, the shape of the crystal reflectivity profile, as well as the natural Lorentzian shape of the atomic line and its Gaussian Doppler broadening to perform high-precision ray-tracing. The reflectivity profile is calculated using the XOP program [79], which uses dynamical diffraction theory from Ref. [80], and the result is checked with the X0H program [81, 82].

A spectrum is obtained by a series of scans of the second crystal. A stepping motor, driven by a micro-stepper, runs continuously, between two predetermined angles that define the angular range of one spectrum. X rays are recorded continuously and stored in a histogram, together with both crystals' temperatures. Successive spectra are recorded in opposite directions. The first crystal is maintained at a fixed angle. Both crystal angles are measured with Heidenhain high-precision angular encoders. The experiment is performed in the following way: a nondispersive-mode (NDM) spectrum is recorded first. Then a dispersive-mode (DM) spectrum is recorded. The sequence is completed with the recording of a second NDM spectrum. Due to the low counting rate, such a sequence of three spectra takes a full day to record. In order to obtain enough statistics, the one-day sequence is repeated typically 7 to 15 times.

III. DATA ANALYSIS

The data analysis is performed in three steps. First we derive a value for the experimental natural width of the line. For this, each experimental dispersive-mode spectrum is fitted with simulated spectra, using an approximate energy (e.g., the theoretical value) and a set of Lorentzian widths. A weighted one-parameter fit is performed on all the results for all recorded dispersive-mode spectra providing a width value and its uncertainty. This experimental width is then used to to generate a new set of simulations, using several different energies and crystal temperatures. These simulations are used to fit each dispersive-mode and nondispersive-mode experimental spectrum in order to obtain the line energy. For each day of data recording this leads to two Bragg angle values, obtained by taking the angular difference between a nondispersive-mode spectrum and a dispersive-mode spectrum:

- one Bragg angle value is obtained by comparing the first nondispersive-mode spectrum of the day and the dispersive-mode spectrum obtained immediately after;

- a second Bragg angle value is obtained by comparing the same dispersive-mode spectrum with the nondispersive-mode spectrum obtained immediately after.

In that way a number of possible time-dependent drifts in the experiment are compensated. We now describe these processes in more detail.

A. Evaluation of the widths

The ion temperature, which is necessary to calculate the Gaussian broadening was obtained by measuring first a line with a completely negligible natural width, the M1 $1s2s\,^3S_1 \rightarrow 1s^2\,^1S_0$, transition. This transition width is $\approx 1 \times 10^{-7}$ eV, which is totally negligible when compared to our spectrometer inherent energy resolution. From this analysis we obtained the Gaussian broadening $\Gamma_{\mathrm{G}}^{\mathrm{Exp.}} = 80.5(46)$ meV [2]. This value also provides the depth of the trapping potential due to the electron space charge. Knowing the experimental Gaussian broadening value $\Gamma_{\mathrm{G}}^{\mathrm{Exp.}}$, we can perform all the needed simulations. For each line under study we then proceed as follows:

- Perform simulations for the dispersive-mode spectra for a set of natural width values Γ_{L}^{i} and the theoretical transition energy E_0 , using the already known $\Gamma_{\mathrm{G}}^{\mathrm{Exp.}}$, and crystal temperature $T_{\mathrm{Ref.}} = 22.5\,^{\circ}\mathrm{C}$;

- Interpolate each simulation result with a piece-wise spline function to obtain a set of continuous, parametrized functions $S_{\left[E_0,\Gamma_{\mathrm{L}}^{i},\Gamma_{\mathrm{G}}^{\mathrm{Exp.}},T\right]}\left(\theta-\theta_0\right)$, where θ_0 correspond to the angle at which the simulation reaches its maximum value, and $T = T_{\mathrm{Ref.}}$;

- Normalize all the functions above to have the same maximum value (we chose the one with $\Gamma_{\mathrm{L}} = 0$ as reference);

- Fit each experimental spectrum with the functions obtained above

$$I\left(\theta-\theta_0, I_{\max}, a, b\right) = I_{\max} S_{\left[E_0,\Gamma_{\mathrm{L}}^{i},\Gamma_{\mathrm{G}}^{\mathrm{Exp.}},T\right]}\left(\theta-\theta_0\right) + a + b\theta, \tag{1}$$

  where $I_{\max}$ is the line intensity, θ the crystal angle, a the background intensity and b the background slope. The parameters θ_0, $I_{\max}$, a and b are adjusted to minimize the reduced $\chi^2\left(\Gamma_{\mathrm{L}}^{i}\right)$. A typical experimental spectrum and the fitted simulated functions, for all the values of Γ_{L}^{i}, are shown in Fig. 1;

- Fit a third degree polynomial to the set of points $[\Gamma_{\mathrm{L}}^{i}, \chi^2\left(\Gamma_{\mathrm{L}}^{i}\right)]$;

- Find the minimum of the third degree polynomial to get the corresponding optimal $\Gamma_{\mathrm{L\,opt.}}^{n}$, n being the experiment run number (see Fig. 2 for an example);

- Get the 68 % error bar $\delta\Gamma^n_{\mathrm{L\,opt.}}$ for experiment run n by finding the values of the width for which [83]

$$\chi^2\left(\Gamma^n_{\mathrm{L\,opt.}} \pm \delta\Gamma^n_{\mathrm{L\,opt.}}\right) = \chi^2\left(\Gamma^n_{\mathrm{L\,opt.}}\right) + 1; \tag{2}$$

- Finally a weighted average of the values in the set of all the $\Gamma^n_{\mathrm{L\,opt.}}$ obtained for all measured spectra is performed to obtain the experimental value $\Gamma^{\mathrm{Exp.}}_{\mathrm{L}}$ and its error bar:

$$\frac{1}{\left(\delta\Gamma^{\mathrm{Exp.}}_{\mathrm{L}}\right)^2} = \sum_n \frac{1}{\left(\Gamma^n_{\mathrm{L\,opt.}}\right)^2}\,,$$
$$\Gamma^{\mathrm{Exp.}}_{\mathrm{L}} = \left(\delta\Gamma^{\mathrm{Exp.}}_{\mathrm{L}}\right)^2 \sum_n \frac{\Gamma^n_{\mathrm{L\,opt.}}}{\left(\Gamma^n_{\mathrm{L\,opt.}}\right)^2}\,. \tag{3}$$

  The sets of $\Gamma^n_{\mathrm{L\,opt.}}$ for both lines studied here are plotted in Fig. 3.

The two first steps are performed by two different methods, one based on the CERN program ROOT, version 6.08 [84–86] and one based on MATHEMATICA, version 11 [87].

B. Transition energy values

Once we obtained the experimental width value $\Gamma^{\mathrm{Exp.}}_{\mathrm{L}}$ of a measured line (cf. Sec. III A), the determination of the correspondent experimental transition energy value E_{exp} is achieved using the following scheme.

- Perform simulations in the nondispersive and dispersive modes for a set of transition energy values $E_k = E_{\mathrm{theo}} + k\Delta E$, where E_{theo} is the theoretical energy value, ΔE an energy increment and k an integer that can take positive or negative values. The simulations are done with the experimental natural width $\Gamma^{\mathrm{Exp.}}_{\mathrm{L}}$ and Gaussian broadening $\Gamma^{\mathrm{Exp.}}_{\mathrm{G}}$. The simulations are performed at various crystal temperature values T_l for each energy.

- As in Sec. III A, interpolate each simulation result with a spline function for both the nondispersive and dispersive modes, to obtain a set of functions depending on all the (E_k, T_l) pairs;

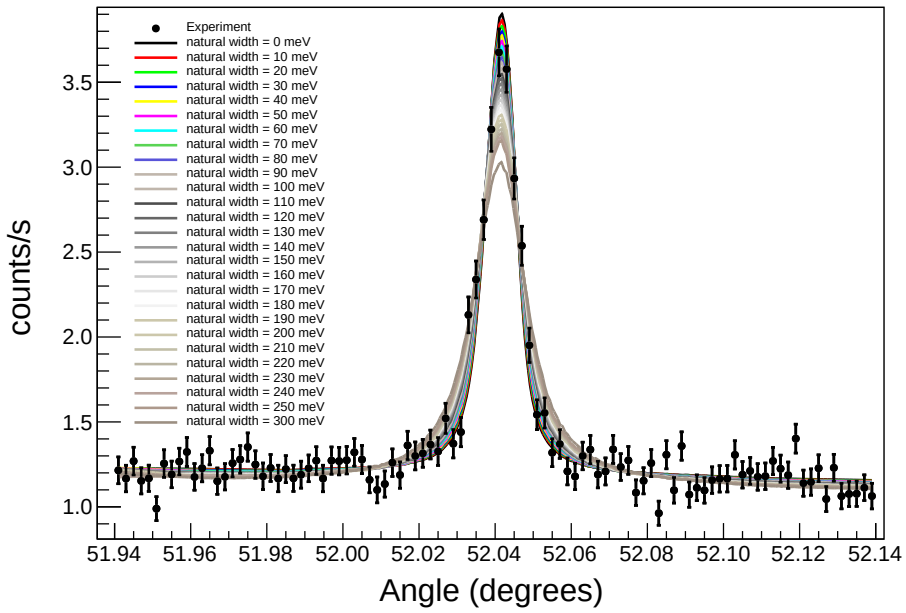

FIG. 1: (Color on line) Example of a dispersive-mode experimental spectrum for the He-like Ar $1s2p\,^1P_1 \rightarrow 1s^2\,^1S_0$ transition (black dots), together with plots of the function in Eq. (1), for different values of the natural line width $\Gamma_{\rm L}^i$. The four parameters have been adjusted to minimize the reduced $\chi^2\,(\Gamma_{\rm L})$ (se text for more explanations).

- Fit each experimental spectrum, using Eq. (1) with $E_0 = E_k$ and $T = T_l$, to obtain the angle difference between the simulation and the experimental spectrum, both in dispersive and nondispersive mode;

- For each pair of dispersive and nondispersive modes experimental spectra, calculate the offsets between simulated spectra $\Delta\theta^{n,k,l}_{\rm Exp.-Simul.} = \left(\theta^{n}_{\rm Exp.DM} - \theta^{n}_{\rm Exp.NDM}\right) - \left(\theta^{k,l}_{\rm Simul.DM} - \theta^{k,l}_{\rm Simul.NDM}\right)$, the experimental value having been obtained in the step above. This offset should be 0 if the energy and temperature used in the simulation were identical to the experimental energy;

- Fit the bidimensional function

$$\Delta\theta_{\rm Exp.-Simul.}(E,T) = p + qE + rE^2 + sET + uT + vT^2, \tag{4}$$

where p, q, r, s, u and v are adjustable parameters, to the set of points $\left[E_k, T_l, \Delta\theta^{n,k,l}_{\rm Exp.-Simul.}\right]$ obtained in the previous step (see Fig. 4 as an example);

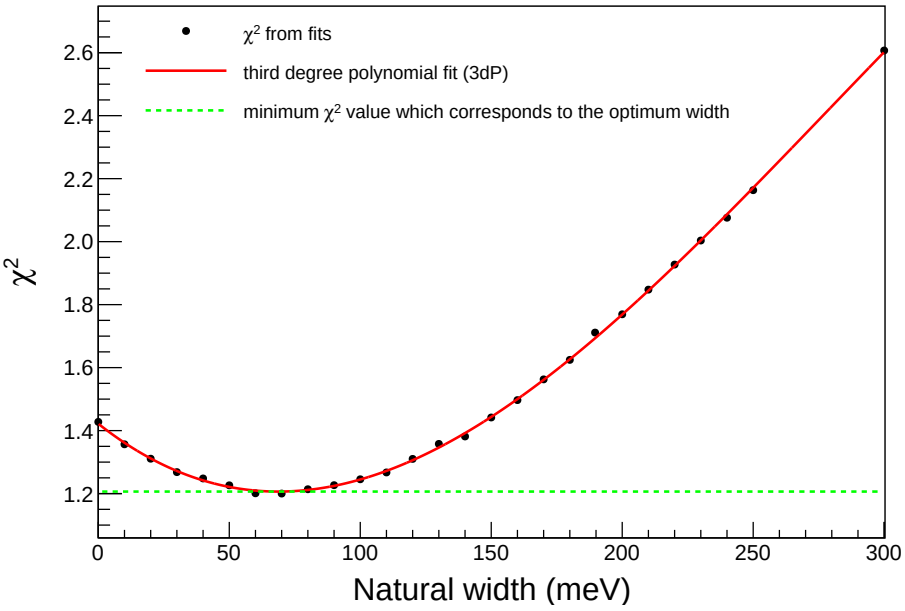

FIG. 2: (Color on line)Third degree polynomial fitted to the $[\Gamma_{\rm L}, \chi^2(\Gamma_{\rm L})]$ set of points (black dots), for the He-like Ar 1s2p $^1P_1 \rightarrow$1s^2 $^1S_0$ transition. The χ^2 values were obtained from the fits represented in Fig. 1 with the different values of $\Gamma_{\rm L}$ presented on the figure.

- The experimental line energy $E^n_{\rm Exp.}$ for spectrum pair number n, is the energy such that $\Delta\theta_{\rm Exp.-Simul.}\left(E^n_{\rm Exp.}, T_{\rm Exp.}\right) = 0$ where $T_{\rm Exp.}$, stands for the average measured temperature on the second crystal;

- As a check, we also used the line energy such that $\Delta\theta_{\rm Exp.-Simul.}\left(E^n_{\rm Exp.}, T_{\rm Ref.}\right) = 0$ ($T_{\rm Ref.}$ =22.5 °C). This leads to a temperature-dependent energy. We then fitted a straight line to the line energy, as a function of the second crystal temperature, and extrapolated to T =22.5 °C. Both methods lead to very close values, well within the uncertainties.

- As in Sec. III A, we plot all pairs $\left(n, E^n_{\rm Exp.}\right)$ and calculate the weighted average to obtain the final experimental energy. The error bar on each point, is a quadratic combination of the instrumental uncertainty, as given in Table I and of the statistical error.

- To check the result, we also plot the pairs $\left(E^n_{\rm Exp.}, T^n_{\rm Exp.}\right)$ and fit them with $E_0 + bT$ to check that there is no residual temperature dependence.

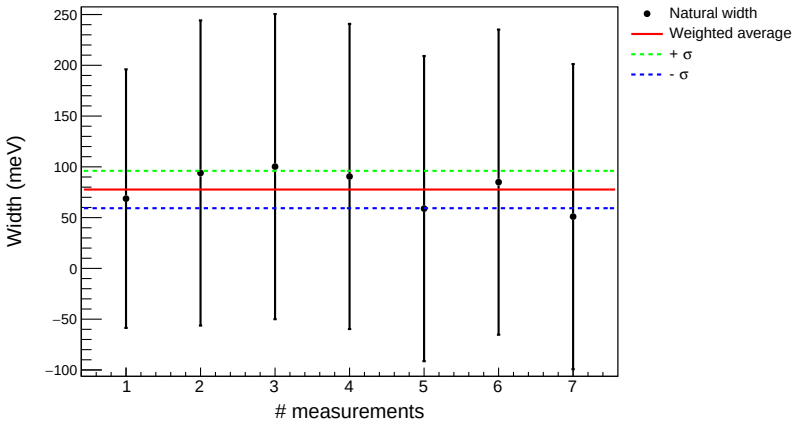

(a) He-like argon $1s2p\,^1P_1 \rightarrow 1s^2\,^1S_0$ transition.

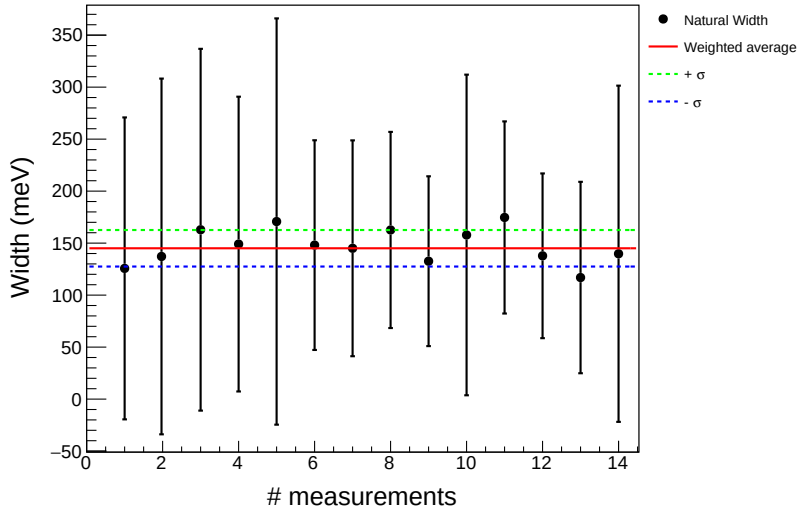

(b) Be-like argon $1s2s^22p\,^1P_1 \rightarrow 1s^22s^2\,^1S_0$ transition.

FIG. 3: (Color on line) Natural width values of all the spectra recorded during the experiment, with weighted average and uncertainties evaluated with Eq. (3).

IV. THEORETICAL CALCULATION

The core-excited $1s2s^22p\,^1P_1 \rightarrow 1s^22s^2\,^1S_0$ transition in Be-like ions has been calculated with the most recent methods, only very recently and only for iron [88], and argon [89]. Previous calculations [90–93] did not take into account QED and relativistic effects to the extent possible today.

For the preparation of this experiment, we performed a calculation of the energy value for the $1s2s^22p\,^1P_1 \rightarrow 1s^22s^2\,^1S_0$ transition in Be-like argon, using the multiconfiguration

TABLE I: Instrumental contributions to the uncertainties in the analysis of the daily experiments (see Refs. [2, 73]).

Contribution:	Value (eV)
Angle encoder error	0.0036
Lattice spacing error	0.00012
Index of refraction	0.0016
Coefficient of thermal expansion	0.00019
X-ray polarization	0.00100
Energy-wavelength correction	0.000078
Temperature (0.5 °C)	0.0040

Dirac-Fock (MCDF) approach as implemented in the in the 2016 version of the general relativistic MCDF code (MCDFGME), developed by Desclaux and Indelicato [94–97]. The full description of the code can be obtained from Refs. [98, 99]. The present version also takes into account the normal and specific mass shifts, evaluated following the method of Shabaev [100–102], as described in [103].

The main advantage of the MCDF approach is the ability to include a large amount of electronic correlation by taking into account a limited number of configurations [104–106]. All calculations were done for a finite nucleus using a uniformly charged sphere. The atomic masses and the nuclear radii were taken from the tables by Audi *et al.* [107] and Angeli and Marinova [67, 108], respectively.

Radiative corrections are introduced from a full QED treatment. The one-electron self-energy is evaluated using the one-electron values of Mohr and co-workers [109–112], and corrected for finite nuclear size [113]. The self-energy screening and vacuum polarization were included using the methods developed by Indelicato and co-workers [95, 96, 114–116]. In previous work, the self-energy screening in this code was based on the Welton approximation [95, 96]. Here we also evaluate the self-energy screening following the model operator approach recently developed by Shabaev *et al.* [71, 117], which has been added to MCDFGME. A detailed description of this new code will be given elsewhere.

Lifetime evaluations are done using the method described in Ref. [118]. The orbitals

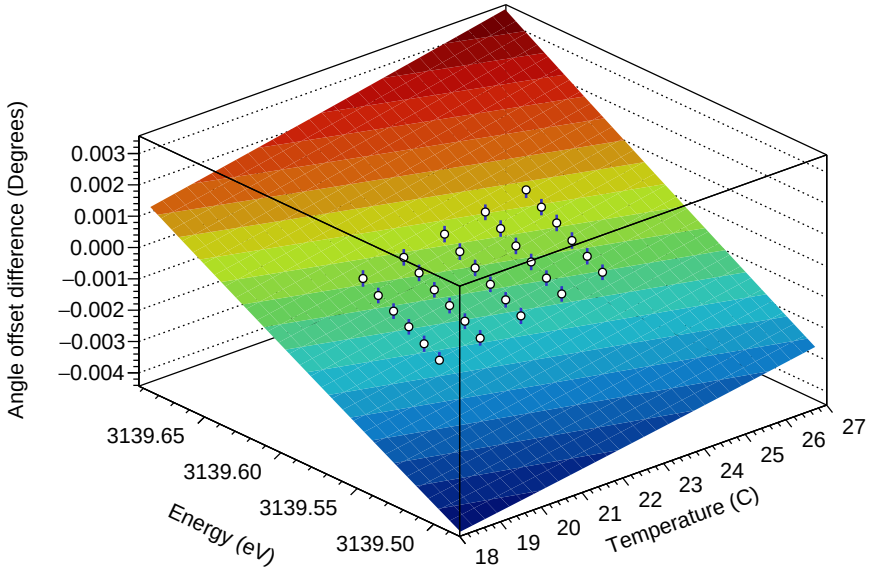

FIG. 4: (Color on line) Fitted two-dimensional function from Eq. (4), and experimental results (white spheres), for the He-like Ar $1s2p\,^1P_1 \rightarrow 1s^2\,^1S_0$ transition. The fit is performed taking into account the statistical error bars in each point.

contributing to the wave function were fully relaxed, and the resulting non-orthogonality between initial and final wave functions fully taken into account, following [119, 120].

The full Breit interaction and the Uehling potential are included in the self-consistent field process. Projection operators have been included [99] to avoid coupling with the negative energy continuum.

As a check, we also performed a calculation of the He-like argon line measured in the present work. Following Refs. [99, 121–123], we use for the excited state the following configurations:

$$\begin{aligned}\left|1s2p\,^1P_1\right\rangle = {} & c_1\left|1s2p, J=1\right\rangle + c_2\left|2s3p, J=1\right\rangle + c_3\left|2p'3d, J=1\right\rangle + c_4\left|3s4p, J=1\right\rangle \\ & + c_5\left|3p'4d, J=1\right\rangle + c_6\left|3d'4f, J=1\right\rangle + c_7\left|4s5p, J=1\right\rangle + c_8\left|4p'5d, J=1\right\rangle \\ & + c_9\left|4d'5f, J=1\right\rangle + c_{10}\left|4f'5g, J=1\right\rangle + c_{11}\left|5s6p, J=1\right\rangle + c_{12}\left|5p'6d, J=1\right\rangle \\ & + c_{13}\left|5d'6f, J=1\right\rangle + c_{14}\left|5f'6g, J=1\right\rangle + c_{15}\left|5g'6h, J=1\right\rangle, \end{aligned} \tag{5}$$

where the l' indicates an orbital with identical angular function as the l one, but with an other radial wave function, for which the orthogonality with orbitals of the same symmetry in other

TABLE II: Total energy and transition energies (in eV) for the $1s2s^22p\,^1P_1 \rightarrow 1s^22s^2\,^1S_0$ transition in Be-like argon, as a function of the maximum principal quantum number n of the correlation orbitals. All correlation from the Coulomb, retardation and QED parts is included. Extrapolation for $n \rightarrow \infty$ is done by fitting the function $a + b/n^2 + c/n^3$ to the correlation energy (Difference with the energy for n and the Dirac-Fock (DF) value) of each level and retaining only the constant term a.

	Welton QED			Model operator QED[71, 117]		
n	Initial	Final	Transition	Initial	Final	Transition
DF	−10313.5818	−7222.7484	3090.8334	−10313.5895	−7222.7520	3090.8375
2	−10319.3248	−7227.3513	3091.9735	−10319.3316	−7227.3548	3091.9767
3	−10320.5339	−7228.6888	3091.8451	−10320.5412	−7228.6922	3091.8490
4	−10320.7554	−7228.9899	3091.7655	−10320.7634	−7228.9934	3091.7700
5	−10320.8781			−10320.8965		
∞	−10320.9135	−7229.1650	3091.748(41)	−10320.9416	−7229.1687	3091.7729(77)

configuration is not enforced. The ground state wave function is taken as usual as $|1s^2\,^1S_0\rangle = c_1\,|1s^2, J=0\rangle + c_2\,|2s^2, J=0\rangle + c_3\,|2p^2, J=0\rangle + \cdots + c_{20}\,|6g^2, J=0\rangle + c_{21}\,|6h^2, J=0\rangle$.

For Be-like argon, the correlation contributions result from the inclusion of all single, double and triple electron excitations of the $n = 1$ and 2 electrons in the unperturbed configuration up to $n = 4$. For the $1s^22s^2\,^1S_0$ ground state it corresponds to 688 configurations and for the $1s2s^22p\,^1P_1$ excited state to 3354 configurations. Convergence for the ground configuration could be obtained in the same way up to $n = 5$, but $n = 4$ was the highest principal quantum numbers that could be dealt with for the core excited one. We performed an estimation of the full correlation energy by doing a fit with the function $a + b/n^2 + c/n^3$, and extrapolation to $n \rightarrow \infty$ for each level, for both the Welton and the Model operator values. The results are presented in Table II. By comparing the extrapolated value and the changes in QED due to the use of either the Welton or effective operator method we estimated the theoretical uncertainty provided in the table.

The Auger width of the $1s2s^22p\,^1P_1$ level is calculated with the MCDFGME code, following Ref. [124] with full relaxation and final-state channel mixing, again taking into account the non-orthogonality between the initial and final state. We use uncorrelated wave functions for these calculations. The results are presented in Table III, together with results from Refs. [92, 125, 126]. The relatively large difference between our present MCDF calculation

TABLE III: Theoretical partial radiative widths, Auger widths and energies for transitions originating from the Be-like $1s2s^22p\,^1P_1$ level. Transition energies are in eV and widths in meV.

		MCDF, Chen (1985) [92]		MCDF, Costa *et al.* 2001 [125]		RCI, Natarajan (2003) [126]	
Initial Level	final level	energy	rate	energy	rate	energy	rate
$1s2s^22p\,^1P_1$	$1s^22s^2\,^1S_0$	3090.66	66.48	3091.95	64.57	3088.958	64.58
$1s2s^22p\,^1P_1$	$1s^22s_{1/2}$	2236.81		2237.03	18.76		
	$1s^22p_{1/2}$	2204.79		2205.19	15.01		
	$1s^22p_{3/2}$	2201.63		2201.82	52.53		
Total Auger			80.30		86.29		
Level width			146.78		150.86		
		MCDF (this work)		FAC (this work)			
		energy	rate	energy	rate		
$1s2s^22p\,^1P_1$	$1s^22s^2\,^1S_0$	3091.80	63.13	3091.11	63.48		
$1s2s^22p\,^1P_1$	$1s^22s_{1/2}$	2240.95	0.52	2241.39	1.13		
	$1s^22p_{1/2}$	2208.95	14.36	2209.22	12.93		
	$1s^22p_{3/2}$	2205.78	48.87	2206.10	43.82		
Total Auger			63.75		57.89		
Level width			126.88		121.36		

and the Dirac-Fock calculation from Ref. [125] , made with an earlier version of our code, is due to correlation and to the evaluation of Auger rates using fully relaxed final state. The contributions of all the other possible transitions to the $1s^2nlJ$ levels, $n = 3 \to \infty$, was evaluated by computing all Auger widths up to $n = 9, l = 8$. The results are presented in Table IV. We then fitted a function $a/n^2 + b/n^3$ to the total Auger width for each principal quantum number n, summing all values of L and J for each value of n, to evaluate the contribution from $n = 10$ up to infinity. We find a =0.056 232 5 meV and b =0.530 28 meV. The total value for the contribution of all levels with $n \geq 3$ is 0.063 meV and is thus negligible.

We have also performed calculations of the transition energies and rates with the "flexible atomic code" (FAC), widely used in plasma physics [127]. This code is based on the relativistic configuration interaction (RCI), with independent particle basis wave functions that are derived from a local central potential. This local potential is derived self-consistently to include the screening of the nuclear potential by the electrons.

TABLE IV: Theoretical Auger widths and energies for transitions from the Be-like $1s2s^22p\,^1P_1$ level to $1s^2nL, J$ levels, $n \geq 3$. Transition energies are in eV and transition widths in meV.

final level	energy	rate	sum for L, J	final level	energy	rate	sum for L, J
$1s^23s_{1/2}$	1723.36	6.720×10^{-4}		$1s^27s_{1/2}$	1397.21	1.724×10^{-4}	
$1s^23p_{1/2}$	1714.51	3.927×10^{-3}		$1s^27p_{1/2}$	1396.79	3.091×10^{-4}	
$1s^23p_{3/2}$	1713.58	1.369×10^{-2}		$1s^27p_{3/2}$	1396.50	1.050×10^{-3}	
$1s^23d_{3/2}$	1710.31	2.750×10^{-3}		$1s^27d_{3/2}$	1396.23	2.690×10^{-4}	
$1s^23d_{5/2}$	1710.01	4.667×10^{-3}	0.0257	$1s^27d_{5/2}$	1396.21	4.471×10^{-4}	
$1s^24s_{1/2}$	1548.43	5.851×10^{-4}		$1s^27f_{5/2}$	1396.19	4.532×10^{-5}	
$1s^24p_{1/2}$	1546.02	1.777×10^{-3}		$1s^27f_{7/2}$	1396.18	6.465×10^{-5}	
$1s^24p_{3/2}$	1544.52	6.030×10^{-3}		$1s^27g_{7/2}$	1396.18	2.734×10^{-6}	
$1s^24d_{3/2}$	1543.07	1.375×10^{-3}		$1s^27g_{9/2}$	1396.17	3.652×10^{-6}	
$1s^24d_{5/2}$	1542.96	2.303×10^{-3}		$1s^27h_{9/2}$	1396.17	5.559×10^{-8}	
$1s^24f_{5/2}$	1542.88	1.271×10^{-4}		$1s^27h_{11/2}$	1396.17	7.098×10^{-8}	
$1s^24f_{7/2}$	1542.81	1.820×10^{-4}	0.0124	$1s^27i_{11/2}$	1396.17	3.138×10^{-10}	
$1s^25s_{1/2}$	1467.29	3.881×10^{-4}		$1s^27i_{13/2}$	1396.17	3.871×10^{-10}	0.0024
$1s^25p_{1/2}$	1466.09	8.848×10^{-4}		$1s^28s_{1/2}$	1380.20	1.208×10^{-4}	
$1s^25p_{3/2}$	1465.31	2.999×10^{-3}		$1s^28p_{1/2}$	1379.92	2.044×10^{-4}	
$1s^25d_{3/2}$	1464.58	7.303×10^{-4}		$1s^28p_{3/2}$	1379.73	6.954×10^{-4}	
$1s^25d_{5/2}$	1464.52	1.218×10^{-3}		$1s^28d_{3/2}$	1379.55	1.801×10^{-4}	
$1s^25f_{5/2}$	1464.47	9.727×10^{-5}		$1s^28d_{5/2}$	1379.54	2.992×10^{-4}	
$1s^25f_{7/2}$	1464.44	1.390×10^{-4}		$1s^28f_{5/2}$	1379.52	3.191×10^{-5}	
$1s^25g_{7/2}$	1464.44	3.071×10^{-6}		$1s^28f_{7/2}$	1379.52	4.550×10^{-5}	
$1s^25g_{9/2}$	1464.42	4.103×10^{-6}	0.0065	$1s^28g_{7/2}$	1379.52	2.156×10^{-6}	
$1s^26s_{1/2}$	1423.50	2.548×10^{-4}		$1s^28g_{9/2}$	1379.51	2.880×10^{-6}	
$1s^26p_{1/2}$	1422.82	4.995×10^{-4}		$1s^28h_{9/2}$	1379.51	5.452×10^{-8}	
$1s^26p_{3/2}$	1422.36	1.695×10^{-3}		$1s^28h_{11/2}$	1379.51	6.961×10^{-8}	
$1s^26d_{3/2}$	1421.94	4.265×10^{-4}		$1s^28i_{11/2}$	1379.51	5.049×10^{-10}	
$1s^26d_{5/2}$	1421.90	7.097×10^{-4}		$1s^28i_{13/2}$	1379.51	6.229×10^{-10}	
$1s^26f_{5/2}$	1421.88	6.618×10^{-5}		$1s^28_{k13/2}$	1379.51	1.467×10^{-12}	
$1s^26f_{7/2}$	1421.86	9.445×10^{-5}		$1s^28_{k15/2}$	1379.50	1.762×10^{-12}	0.0016
$1s^26g_{7/2}$	1421.86	3.265×10^{-6}		Total			0.0522
$1s^26g_{9/2}$	1421.85	4.361×10^{-6}		Extrapollated to $n \to \infty$			0.0631
$1s^26h_{9/2}$	1421.85	4.146×10^{-8}					
$1s^26h_{11/2}$	1421.84	5.293×10^{-8}	0.0038				

TABLE V: Measured and computed natural line width values for the $1s2p\,^1P_1 \rightarrow 1s^2\,^1S_0$ transitions in He-like Ar. All values are given in meV, and estimated uncertainties are shown in parentheses.

Transition	Experiment	Theory	Reference
$1s2p\,^1P_1 \rightarrow 1s^2\,^1S_0$	78 (18)	70.43	Johnson *et al.* (1995) [129]
		70.4778 (25)	MCDF (this work)
		70.49 (14)	Drake (1979) [128]

V. RESULTS AND COMPARISON WITH THEORY FOR THE HE-LIKE $1s2p\,^1P_1 \rightarrow 1s2s\,^1S_0$ TRANSITION

A. Line widths

The values for the line widths, obtained as explained in Sec. III A and Fig. 3a, are presented in Table V, together with several theoretical results. There are several possible E1 radiative transitions originating from the $1s2p\,^1P_1$ level. Because of the large energy difference, the contribution of the $1s2p\,^1P_1 \rightarrow 1s^2\,^1S_0$ transition to the level width is strongly dominant. The next largest contribution, due to the the $1s2p\,^1P_1 \rightarrow 1s2s\,^1S_0$ transition, contributes only 0.0001 meV to the 70.4 meV width. The width of the $n = 2 \rightarrow n = 1$ transitions has been calculated using Drake's unified method [128], relativistic random phase approximation, MCDF, relativistic configuration interaction (RCI) and QED [129]. The effect of the negative energy continuum has been discussed in Refs. [123, 130]. Radiative corrections to the photon emission have also been evaluated [131]. The agreement between all theoretical values and our measurement always well within the experimental error bar.

B. Transition energies

We present in Fig. 5 the transition energy values obtained from the successive pairs of dispersive and nondispersive-modes spectra, recorded during the experiment for the He-like argon $1s2p\,^1P_1 \rightarrow 1s^2\,^1S_0$ following the method presented in Sec. III. The weighted average and $\pm 1\sigma$ bands are plotted as well.

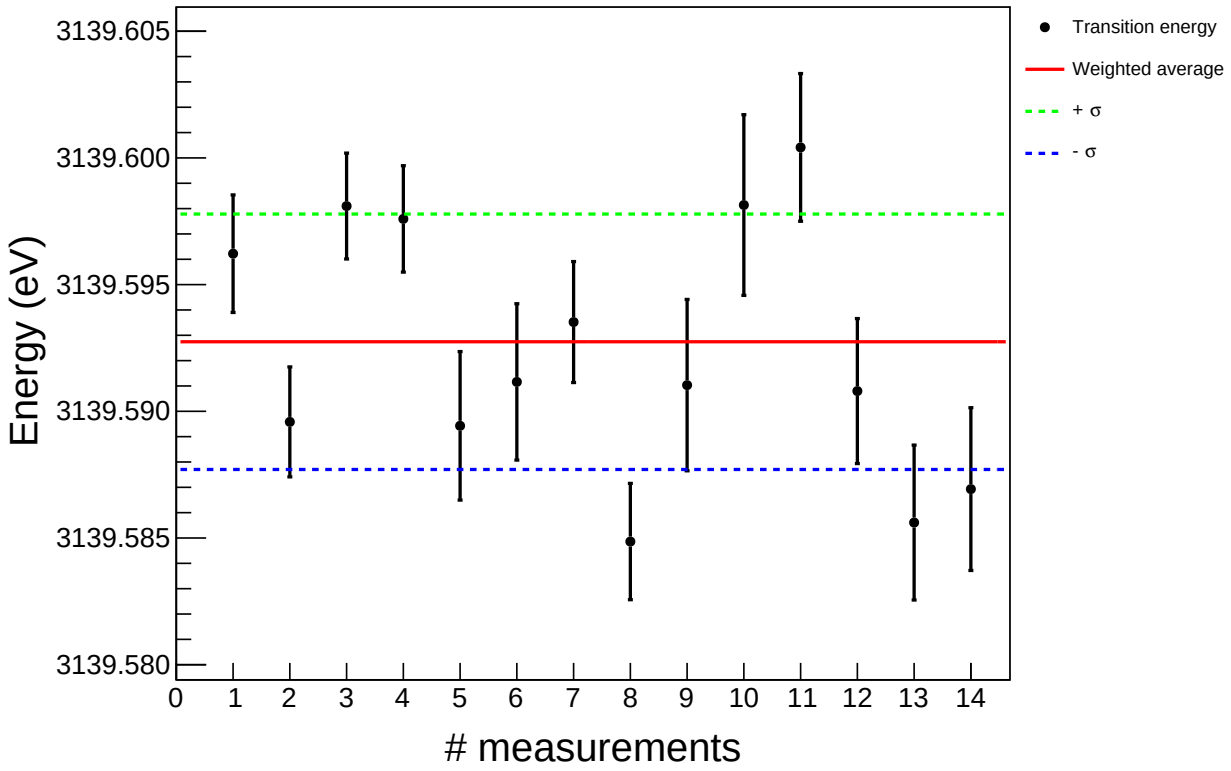

FIG. 5: (Color on line) He-like argon $1s2p\,^1P_1 \rightarrow 1s^2\,^1S_0$ transition energy values of the different spectra recorded during the experiment. Error bars correspond to statistical uncertainty. Every pair of points correspond to one-day data taking (see text for explanations).

Table VI presents the measured He-like argon $1s2p\,^1P_1 \rightarrow 1s^2\,^1S_0$ transition energy, together with all known experimental and theoretical results. The final experimental accuracy, combining the instrumental contributions from Table I is 2.42×10^{-6}. The value is in agreement with a preliminary result, obtained with the same set-up, but using fit with Voigt profiles of both the experimental spectra and the simulations[132, 133]. The agreement with the most precise experiments, *i.e.*, the two reference-free experiment [1, 43] and the recoil ion experiment of Deslattes *et al.* [39] is well within combined error bars. The agreement with the calculation of Artemyev *et al.* [54], the present calculation performed with effective self-energy operators and most recent calculation is also within combined error bars.

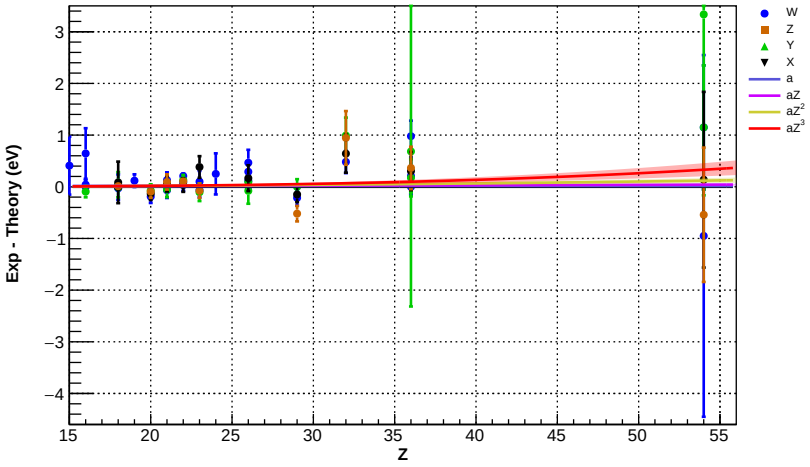

(a) All Z-range.

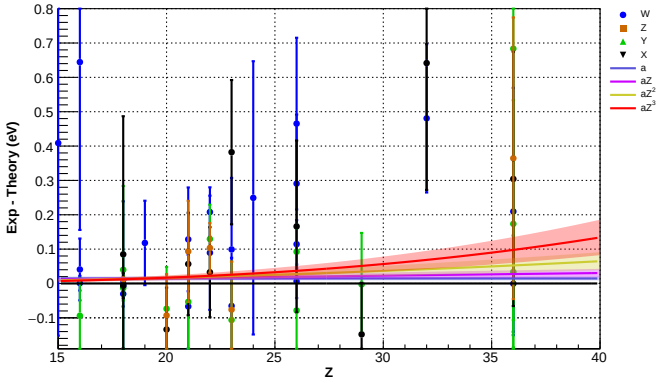

(b) (Color on line) Zoom on the $15 \leq Z \leq 40$-range, and small energy differences.

FIG. 6: (Color on line) Comparison between the theoretical values by Artemyev *et al.* [54] and experimental data for $n = 2 \rightarrow n = 1$ transition in He-like ions presented in Tables VII and VIII for $12 \leq Z \leq 54$. The continuous lines represent the weighted fit with a, aZ, aZ^2 and aZ^3 functions, and the shaded area the $\pm 1\sigma$ bands, representing the 68 % confidence interval from the fit. The deviation is always lower than $\pm 2\sigma$ and thus is not significant. From this we cannot conclude in favor of a systematic Z dependent deviation.

C. Comparison between measurements and calculations for $12 \leq Z \leq 92$

There has been many measurements of $n = 2 \rightarrow n = 1$ transition energies in He-like ions. The reference-free measurements, of the kind reported in the present work, and the

measurements calibrated against x-ray standards or transitions in H-like ions are summarized in Tables VII and VIII for $7 \leq Z \leq 92$. Relative measurements, using the theoretical value for one of the He-like line in the spectrum, originating from ECRIS or tokamak experiments are summarized in Table IX. When older calculations were used as a reference, we used the energies of Ref. [54] to obtain an updated value for this table.

A detailed analysis of the difference between theory [54] and experiment has been performed in previous work [3, 5, 8]. Here we provide an updated analysis, which include our new result and the data from Tables VII and VIII .

The differences between these experimental values and Artemyev *et al.* [54] theoretical values are plotted in Fig. 6 together with weighted fits by several functions of the shape aZ^n, $n = 0$ to 3. The 1σ error bands for the fits are also plotted. These error bands show that there is no significant deviation between theory and experiment.

In order to reinforce this conclusion, we have performed a systematic significance analysis. This analysis has been performed fitting functions of the form $f(Z) = aZ^n$, $n = 0$, 12 on three datasets build using the data presented in Tables VII and VIII. One data set contains only the w transition, one contains all w, x, y, and z transitions, and the last one is the same, from which the experimental values of this work, of Kubiçek *et al.* [7] and of Amaro *et al.* [2] have been removed. The values of the reduced χ^2 are plotted as a function of n in Fig. 7 for the three subsets. It should be noted that the χ^2 increases as a function of n, although in two of the subsets there is a weak local minimum. We present in Fig. 8 the uncertainty of the fit coefficient a in standard-error units as a function of n for all three datasets. The figure shows that the maximum deviation from zero is obtained for $n = 0$. It can be noticed that the deviation of the fit coefficient tends to zero with increasing value of n while the reduced-χ^2 increases. For the other two datasets considered, i.e., all experimental values presented in Tables VII and VIII or considering the subset of the w-lines, there is a local maximum for each dataset. For all experimental data the local maximum happens at $n \simeq 4.2$ with a coefficient significance of 3.5 standard errors, while for the w-lines the local maximum is at $n \simeq 3.8$ with a deviation of 3 standard errors from zero. Although the presence of this local maximum for different monomial orders of n, the maximum deviation from zero of the fit parameter is at $n = 0$ as well as the minimum reduced-χ^2 value. This leads to the conclusion that the $f(Z) = aZ^0$ is the most probable model to describe the data when considering a power law dependence with Z.

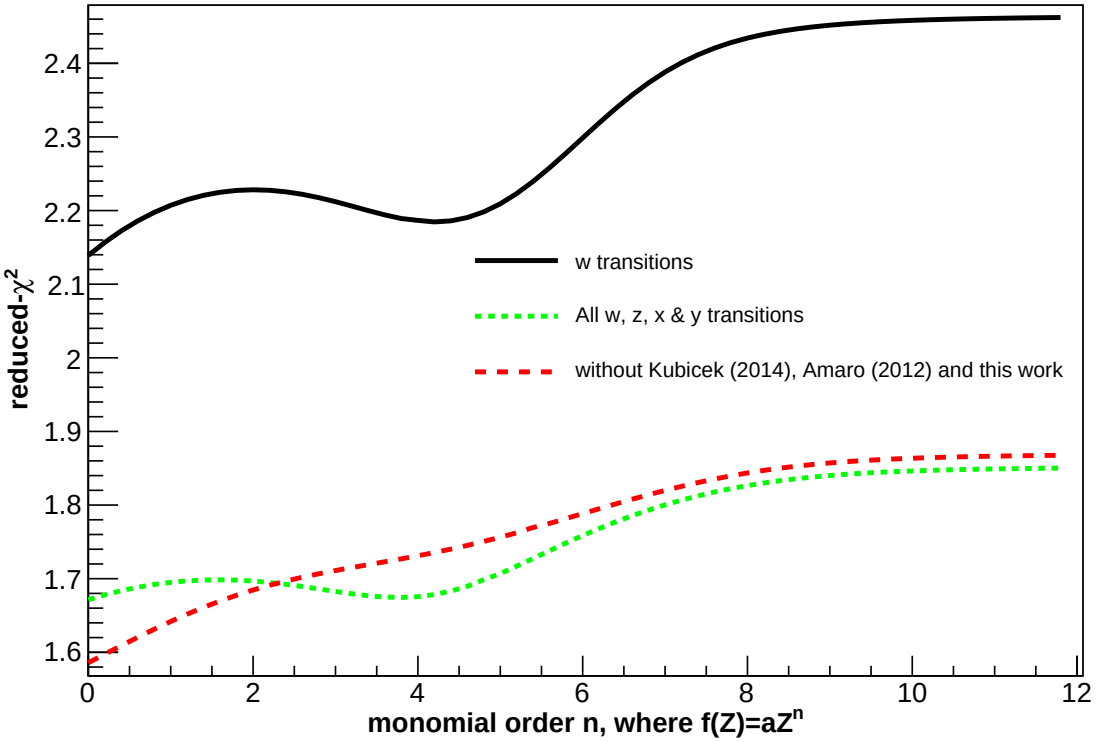

FIG. 7: (Color on line) Values of the reduced χ^2 function as a function of n, when fitting aZ^n, $n = 0$ to 12, to the experiment-theory differences from Tables VII and VIII. Dotted line: reduced χ^2 fitting all 4 w, x, y, z transitions energies differences with theory. Dotted line: reduced χ^2 fitting only the $1s2p\,^1P_1 \rightarrow 1s^2\,^1S_0$ (w) values. Dashed line: fit to all transitions values, removing the reference-free values from this work and from Refs. [2, 7].

To sustain this conclusion, a χ^2 goodness of a fit test was performed. Fig. 9 shows the result probability (p-value) of the χ^2 cumulative distribution function (upper tail) as a function of n, for the given degrees of freedom and the minimum χ^2 value of each performed fit. It can be noticed that the highest p-value for the three considered datasets is for $n = 0$, and, as before, one can see a local maximum when considering all experimental results from Tables VII and VIII or just the w-lines for the same n value as from the Fig. 8. Considering the standard significance level of 0.05 to evaluate the acceptance or rejection of the null hypotheses, and since the highest p-value is 0.002 for the three considered datasets, the null hypotheses cannot be accepted. Therefore, we conclude that we cannot claim that there is a dependence of Z of the form $f(Z) = aZ^n$ for any given n with $0 \leq n \leq 12$.

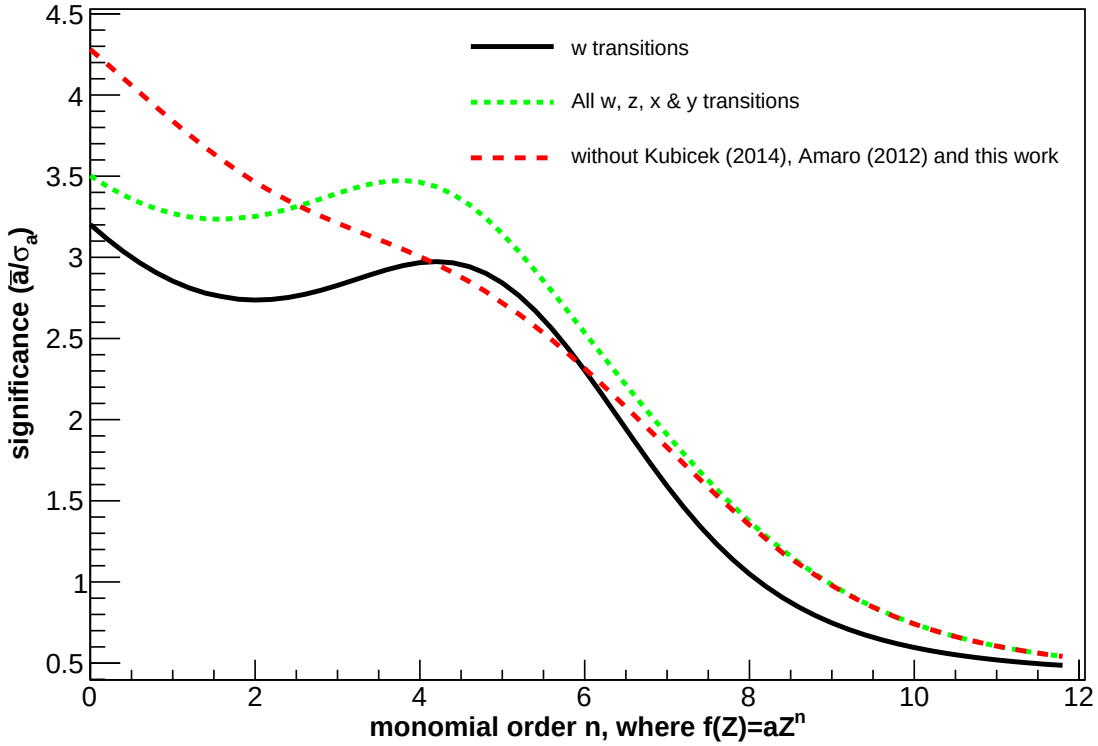

FIG. 8: (Color on line) Values of the significance of the fit coefficient in standard-error units as a function of n when fitting aZ^n to the experiment-theory differences from Tables VII and VIII.

VI. RESULTS AND COMPARISON WITH THEORY FOR THE BE-LIKE $1s2s^22p\,^1P_1 \rightarrow 1s^22s^2\,^1S_0$ TRANSITION

The width of the $1s2s^22p\,^1P_1$ in contrast to the He-like case, has both radiative and non-radiative (Auger) contributions. The radiative part is also heavily dominated by the $1s2s^22p\,^1P_1 \rightarrow 1s^22s^2\,^1S_0$ transition. As seen in Table III, the non-radiative part is mostly due to three Auger transitions, the $1s2s^22p\,^1P_1 \rightarrow 1s^22s\,^2S_{1/2}$, the $1s2s^22p\,^1P_1 \rightarrow 1s^22p\,^2P_{1/2}$ and the $1s2s^22p\,^1P_1 \rightarrow 1s^22p\,^2P_{3/2}$. The radiative and non-radiative contributions are of similar size. The distribution of results for the daily experiments are presented in Fig. 3a. Our experimental width and the comparison with theory are presented in Table X. The agreement between theory and experiment is within combined experimental and theoretical uncertainty.

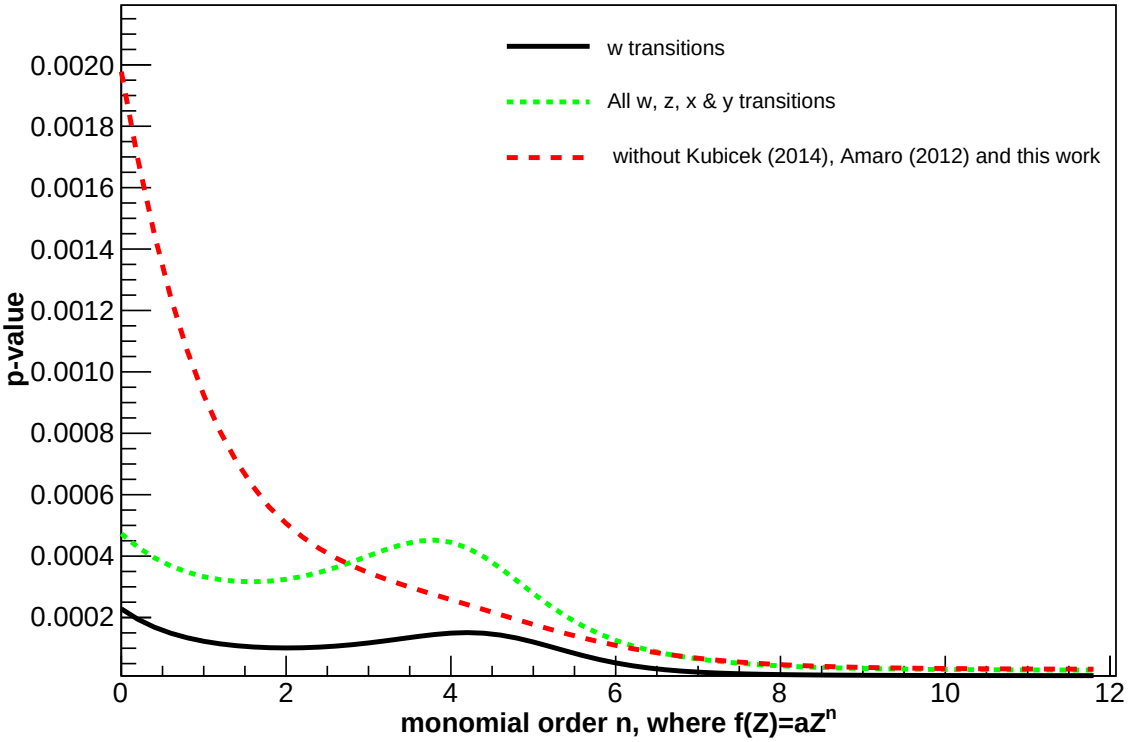

FIG. 9: (Color on line) p-value as a function of n when fitting aZ^n to the experiment-theory differences from Tables VII and VIII.

We present in Fig. 10 the transition energy values obtained from the successive pairs of dispersive and nondispersive-modes spectra, recorded during the experiment for the Be-like argon $1s2s^22p\,^1P_1 \rightarrow 1s^22s^2\,^1S_0$, following the method presented in Sec. III. The weighted average and $\pm 1\sigma$ values are plotted as well.

In Table XI, we present our results for the $1s2s^22p\,^1P_1 \rightarrow 1s^22s^2\,^1S_0$ transition energies. The measurement has been performed with a relative uncertainty of 2.7×10^{-6}. The difference with Yerokhin *et al.* calculation [89], which is given with a relative accuracy of 11×10^{-6} is 9.7×10^{-6}. The difference with our MCDF results using effective operators self-energy screening is 2.3×10^{-6}, while it is 3.6×10^{-6} with the calculation using the Welton method. The difference between the present reference-free measurement and the relative measurement presented in Ref. [52], calibrated against the theoretical value of the $1s2s\,^3S_1 \rightarrow 1s^2\,^1S_0$ transition energy of [54] is only 0.4×10^{-6}. All recent measurement and calculation are thus forming a very coherent set of data.

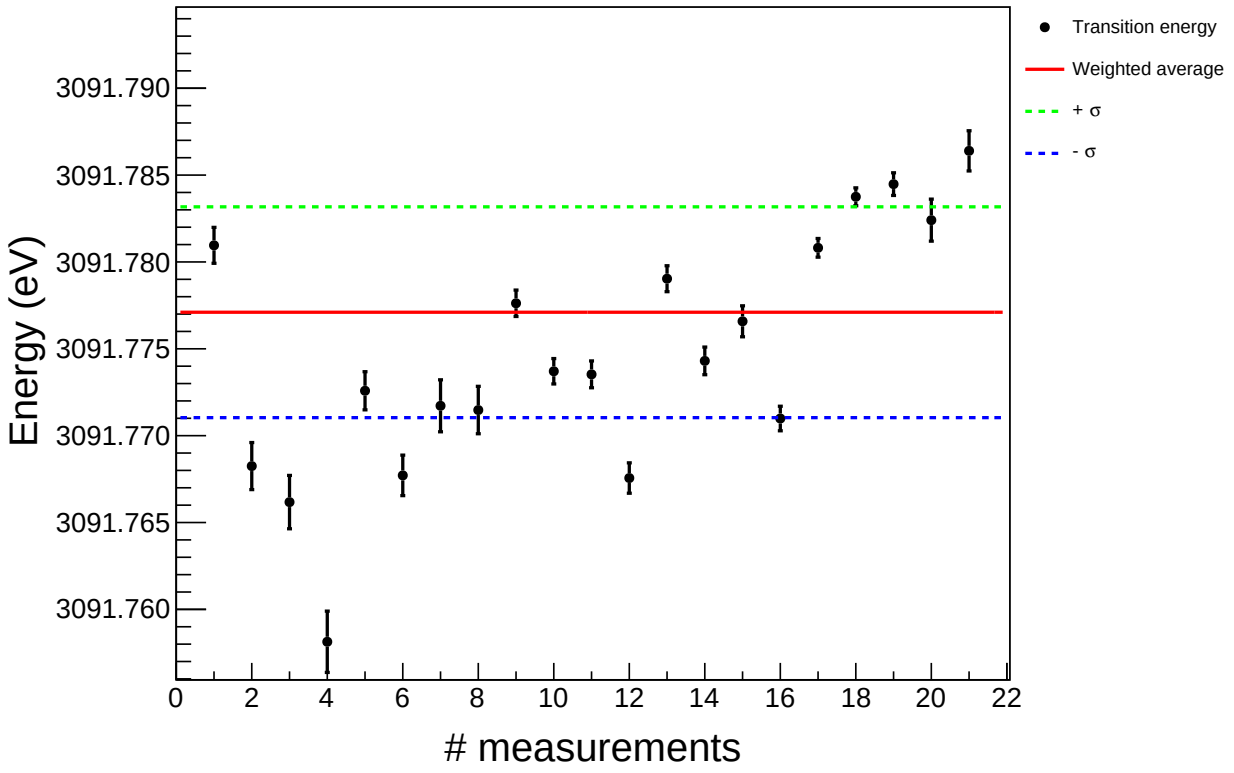

FIG. 10: (Color on line) Be-like argon $1s2s^22p\,^1P_1 \rightarrow 1s^22s^2\,^1S_0$ transition energy values for the different spectra recorded during the experiment. Error bars correspond to statistical uncertainty. Every pair of points correspond to one-day data taking (see text for explanations).

The energy of this transition has not been extensively studied. It was measured relative to either theoretical value in S, Cl and Ar [52], Sc [48], Fe [51, 151], Ni [41] and Pr [152] or to K-edges in Fe [4]. The width and Auger rate for this transition have also been measured in iron [4, 153], with the combined use of synchrotron radiation and ion production with an EBIT. In Fig. 11, we present a comparison between theory and experiment, and between different calculations for the $1s2s^22p\,^1P_1 \rightarrow 1s^22s^2\,^1S_0$ line energy, for $10 \leq Z \leq 29$. Since there is no recent calculation covering all elements for which there is an experimental, we use as reference the old calculation from Ref. [91], which does not include accurate QED corrections.

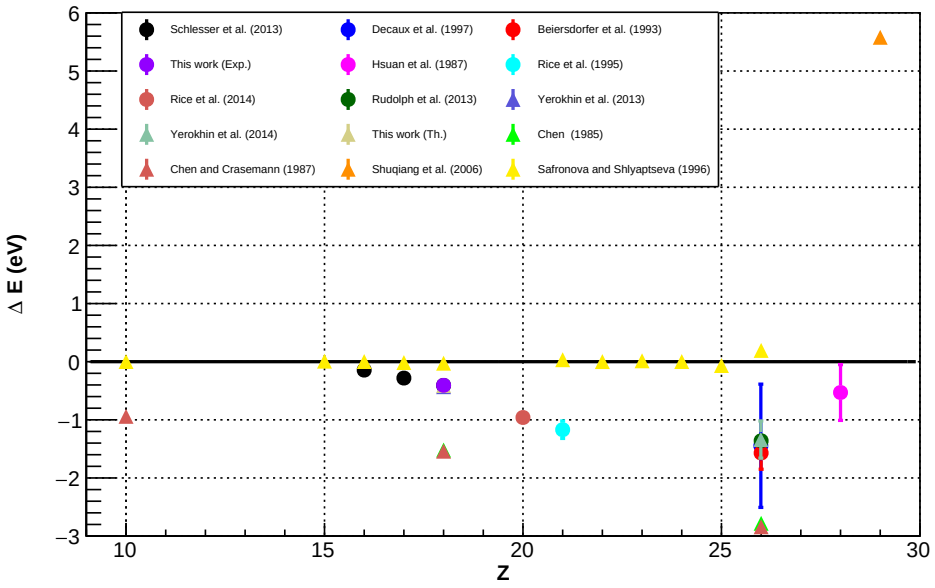

FIG. 11: (Color on line) Comparison between experimental and theoretical values for the $1s2s^22p\,^1P_1 \rightarrow 1s^22s^2\,^1S_0$ transition energies, as a function of Z. Round dots represents experimental results and triangular ones theoretical results. All values are compared to the energies in Ref. [91]. Experimental results references: Schlesser *et al.* (2013) [52], Beiersdorfer *et al.* (1993) [51], Decaux *et al.* (1997) [151], Rudolph *et al.* (2013) [4], Hsuan *et al.* (1987) [41], Rice *et al.* (1995) [48], Rice *et al.* (2014) [49]. Theoretical results references: Yerokhin *et al.* (2015) [89], Yerokhin *et al.* (2014) [88], Chen and Crasemann (1987) [93], Chen (1985) [92], Shuqiang *et al.* (2006) [156], Safronova and Shlyaptseva (1996) [154].

VII. CONCLUSIONS

In the present work, we report the reference-free measurement of two x-ray line transition energies and widths in He-like ($1s2p\,^1P_1 \rightarrow 1s^2\,^1S_0$) and Be-like ($1s2s^22p\,^1P_1 \rightarrow 1s^22s^2\,^1S_0$) argon ions. The measurement of the energy of the $1s2s^22p\,^1P_1 \rightarrow 1s^22s^2\,^1S_0$ transition is the first reference-free measurement for a transition for an ion with more than two-electrons. The measurements were made with a double-crystal spectrometer connected to an ECRIS. The data analysis was performed using a dedicated x-ray tracing simulation code that includes the physical characteristics and geometry of the detector. The energy measurements agree within the error bars with the most accurate calculations and with the more recent measurements.

We have also performed MCDF calculations of the transition energies and widths, using both the MCDFGME code, with improved self-energy screening and the RCI flexible atomic code FAC and compared with all existing theoretical and experimental results available to us. The MCDFGME theoretical results are in agreement with existing experimental results and with the most advanced calculations available.

We have analyzed the difference between all available $n = 2 \rightarrow n = 1$ experimental transition energies in He-like ions for $Z \geq 12$ and the theoretical results from Ref. [54]. When taking into account the recent high-precision, reference-free measurements in heliumlike argon [1, 2, 7] and the present result, in He-like iron[4], and in He-like krypton[9] from the Heidelberg and Paris groups, as well as the copper result [8] by the Livermore group, we have shown that there is no significant Z-dependent deviation between the most advanced theory and experiment.

The method presented here will be extended to other charge-states like lithium-like or boron-like ions, and nearby elements in the near future.

ACKNOWLEDGMENTS

This research was supported in part by the projects No. PEstOE/FIS/UI0303/2011, PTDC/FIS/117606/2010, and by the research centre grant No. UID/FIS/04559/2013 (LIBPhys), from FCT/MCTES/PIDDAC, Portugal. P.A., J.M., and M.G. acknowledge support from FCT, under Contracts No. SFRH/BPD/92329/2013, No. SFRH/BD/52332/2013, and No. SFRH/BPD/92455/2013 respectively. Laboratoire Kastler Brossel (LKB) is "Unité Mixte de Recherche de Sorbonne University-UPMC, de ENS-PSL Research University, du Collge de France et du CNRS n° 8552". P.I. is a member of the Allianz Program of the Helmholtz Association, contract n° EMMI HA-216 "Extremes of Density and Temperature: Cosmic Matter in the Laboratory". The SIMPA ECRIS has been financed by grants from CNRS, MESR, and UPMC. The experiment has been supported by grants from BNM 01 3 0002 and the ANR ANR-06-BLAN-0223. We thank Dr. Martino Trassinelli (INSP) for

valuable discussions and his help during some stage of the experiment.

---

[1] H. Bruhns, J. Braun, K. Kubiçek, J. R. Crespo López-Urrutia, and J. Ullrich, Phys. Rev. Lett. **99**, 113001 (2007).

[2] P. Amaro, S. Schlesser, M. Guerra, E. Le Bigot, J.-M. Isac, P. Travers, J. P. Santos, C. I. Szabo, and P. Indelicato, Phys. Rev. Lett. **109**, 043005 (2012).

[3] C. T. Chantler, M. N. Kinnane, J. D. Gillaspy, L. T. Hudson, A. T. Payne, L. F. Smale, A. Henins, J. M. Pomeroy, J. N. Tan, J. A. Kimpton, et al., Phys. Rev. Lett. **109**, 153001 (2012), URL `http://link.aps.org/doi/10.1103/PhysRevLett.109.153001`.

[4] J. K. Rudolph, S. Bernitt, S. W. Epp, R. Steinbrügge, C. Beilmann, G. V. Brown, S. Eberle, A. Graf, Z. Harman, N. Hell, et al., Phys. Rev. Lett. **111**, 103002 (2013).

[5] C. T. Chantler, A. T. Payne, J. D. Gillaspy, L. T. Hudson, L. F. Smale, A. Henins, J. A. Kimpton, and E. Takács, New J. Phys. **16**, 123037 (2014).

[6] A. T. Payne, C. T. Chantler, M. N. Kinnane, J. D. Gillaspy, L. T. Hudson, L. F. Smale, A. Henins, J. A. Kimpton, and E. Takacs, J. Phys. B: At. Mol. Opt. Phys. **47**, 185001 (2014), URL `http://stacks.iop.org/0953-4075/47/i=18/a=185001`.

[7] K. Kubiçek, P. H. Mokler, V. Mäckel, J. Ullrich, and J. R. Crespo López-Urrutia, Phys. Rev. A **90**, 032508 (2014), URL `http://link.aps.org/doi/10.1103/PhysRevA.90.032508`.

[8] P. Beiersdorfer and G. V. Brown, Phys. Rev. A **91**, 032514 (2015), URL `http://link.aps.org/doi/10.1103/PhysRevA.91.032514`.

[9] S. W. Epp, R. Steinbrügge, S. Bernitt, J. K. Rudolph, C. Beilmann, H. Bekker, A. Müller, O. O. Versolato, H. C. Wille, H. Yavaş, et al., Phys. Rev. A **92**, 020502 (2015), URL `http://link.aps.org/doi/10.1103/PhysRevA.92.020502`.

[10] S. Sturm, A. Wagner, B. Schabinger, J. Zatorski, Z. Harman, W. Quint, G. Werth, C. H. Keitel, and K. Blaum, Phys. Rev. Lett. **107**, 023002 (2011), URL `http://link.aps.org/doi/10.1103/PhysRevLett.107.023002`.

[11] A. Wagner, S. Sturm, F. Köhler, D. A. Glazov, A. V. Volotka, G. Plunien, W. Quint, G. Werth, V. M. Shabaev, and K. Blaum, Phys. Rev. Lett. **110**, 033003 (2013), URL `http://link.aps.org/doi/10.1103/PhysRevLett.110.033003`.

[12] S. Sturm, F. Kohler, J. Zatorski, A. Wagner, Z. Harman, G. Werth, W. Quint, C. H. Keitel,

and K. Blaum, Nature **506**, 467 (2014), URL http://dx.doi.org/10.1038/nature13026.

[13] F. Köhler, S. Sturm, A. Kracke, G. Werth, W. Quint, and K. Blaum, J. Phys. B: At. Mol. Opt. Phys. **48**, 144032 (2015), URL http://stacks.iop.org/0953-4075/48/i=14/a=144032.

[14] J. Ullmann, Z. Andelkovic, A. Dax, W. Geithner, C. Geppert, C. Gorges, M. Hammen, V. Hannen, S. Kaufmann, K. König, et al., J. Phys. B: At. Mol. Opt. Phys. **48**, 144022 (2015), URL http://stacks.iop.org/0953-4075/48/i=14/a=144022.

[15] J. P. Marques, P. Indelicato, F. Parente, J. M. Sampaio, and J. P. Santos, Phys. Rev. A **94**, 042504 (2016).

[16] V. A. Yerokhin, E. Berseneva, Z. Harman, I. I. Tupitsyn, and C. H. Keitel, Phys. Rev. A **94**, 022502 (2016), URL http://link.aps.org/doi/10.1103/PhysRevA.94.022502.

[17] P. Beiersdorfer, A. L. Osterheld, J. H. Scofield, J. R. Crespo Lpez-Urrutia, and K. Widmann, prl **80**, 3022 (1998), URL http://journals.aps.org/prl/abstract/10.1103/PhysRevLett.80.3022.

[18] P. Seelig, S. Borneis, A. Dax, T. Engel, S. Faber, M. Gerlach, C. Holbrow, G. Huber, T. Khl, D. Marx, et al., Phys. Rev. Lett. **81**, 4824 (1998).

[19] S. Boucard and P. Indelicato, Eur. Phys. J. D **8**, 59 (2000).

[20] P. Beiersdorfer, S. B. Utter, K. L. Wong, J. R. C. Lpez-Urrutia, J. A. Britten, H. Chen, C. L. Harris, R. S. Thoe, D. B. Thorn, E. Trbert, et al., pra **64**, 032506 (2001).

[21] V. A. Yerokhin and V. M. Shabaev, Phys. Rev. A **64**, 012506 (2001).

[22] V. M. Shabaev, A. N. Artemyev, V. A. Yerokhin, O. M. Zherebtsov, and G. Soff, Phys. Rev. Lett. **86**, 3959 (2001).

[23] A. V. Volotka, D. A. Glazov, O. V. Andreev, V. M. Shabaev, I. I. Tupitsyn, and G. Plunien, Phys. Rev. Lett. **108**, 073001 (2012), URL http://link.aps.org/doi/10.1103/PhysRevLett.108.073001.

[24] O. V. Andreev, D. A. Glazov, A. V. Volotka, V. M. Shabaev, and G. Plunien, Phys. Rev. A **85**, 022510 (2012), URL http://link.aps.org/doi/10.1103/PhysRevA.85.022510.

[25] W. Nörtershuser, M. Lochmann, R. Jöhren, C. Geppert, Z. Andelkovic, D. Anielski, B. Botermann, M. Bussmann, A. Dax, N. Frömmgen, et al., Physica Scripta **2013**, 014016 (2013), URL http://stacks.iop.org/1402-4896/2013/i=T156/a=014016.

[26] M. Lochmann, R. Jöhren, C. Geppert, Z. Andelkovic, D. Anielski, B. Botermann, M. Bussmann, A. Dax, N. Frömmgen, M. Hammen, et al., pra **90**, 030501 (2014), URL http:

//link.aps.org/doi/10.1103/PhysRevA.90.030501.

[27] P. Beiersdorfer, E. Trbert, G. V. Brown, J. Clementson, D. B. Thorn, M. H. Chen, K. T. Cheng, and J. Sapirstein, Phys. Rev. Lett. **112**, 233003 (2014), URL http://link.aps.org/doi/10.1103/PhysRevLett.112.233003.

[28] J. Vollbrecht, Z. Andelkovic, A. Dax, W. Geithner, C. Geppert, C. Gorges, M. Hammen, V. Hannen, S. Kaufmann, K. König, et al., Journal of Physics: Conference Series **583**, 012002 (2015), URL http://stacks.iop.org/1742-6596/583/i=1/a=012002.

[29] J. Ullmann, Z. Andelkovic, C. Brandau, A. Dax, W. Geithner, C. Geppert, C. Gorges, M. Hammen, V. Hannen, S. Kaufmann, et al., **8**, 15484 (2017), URL http://dx.doi.org/10.1038/ncomms15484.

[30] R. Pohl, A. Antognini, F. Nez, F. D. Amaro, F. Biraben, J. M. R. Cardoso, D. S. Covita, A. Dax, S. Dhawan, L. M. P. Fernandes, et al., Nature **466**, 213 (2010), URL http://www.nature.com/doifinder/10.1038/nature09250.

[31] A. Antognini, F. Nez, K. Schuhmann, F. D. Amaro, F. Biraben, J. M. R. Cardoso, D. S. Covita, A. Dax, S. Dhawan, M. Diepold, et al., Science **339**, 417 (2013), URL http://www.sciencemag.org/content/339/6118/417.abstract.

[32] R. Pohl, F. Nez, L. M. P. Fernandes, F. D. Amaro, F. Biraben, J. M. R. Cardoso, D. S. Covita, A. Dax, S. Dhawan, M. Diepold, et al., Science **353**, 669 (2016), URL http://science.sciencemag.org/content/sci/353/6300/669.full.pdf.

[33] E. V. Aglitskii, V. A. Boiko, S. M. Zakharov, S. A. Pikuz, and A. Y. Faenov, Soviet Journal of Quantum Electronics **4**, 500 (1974), URL http://stacks.iop.org/0049-1748/4/i=4/a=R16.

[34] H. D. Dohmann and R. Mann, Zeit. für Phys. A **291**, 15 (1979).

[35] J. P. Briand, J. P. Mosse, P. Indelicato, P. Chevallier, D. Girard-Vernhet, A. Chetiouy, M. T. Ramos, and J. P. Desclaux, Phys. Rev. A **28**, 1413 (1983).

[36] T. Stöhlker, P. H. Mokler, K. Beckert, F. Bosch, H. Eickhoff, B. Franzke, H. Geissel, M. Jung, T. Kandler, O. Klepper, et al., Nuclear Instruments and Methods in Physics Research B **87**, 64 (1994).

[37] T. Stöhlker, P. H. Mokler, F. Bosch, R. W. Dunford, F. Franzke, O. Klepper, C. Kozhuharov, T. Ludziejewski, F. Nolden, H. Reich, et al., Phys. Rev. Lett. **85**, 3109 (2000).

[38] A. Gumberidze, T. Stöhlker, D. Banaś, K. Beckert, P. Beller, H. F. Beyer, F. Bosch,

S. Hagmann, C. Kozhuharov, D. Liesen, et al., Phys. Rev. Lett. **94**, 223001 (2005), URL http://link.aps.org/doi/10.1103/PhysRevLett.94.223001.

[39] R. D. Deslattes, H. F. Beyer, and F. Folkmann, J. Phys. B: At. Mol. Phys. **17**, L689 (1984).

[40] M. Bitter, K. W. Hill, M. Zarnstorff, S. von Goeler, R. Hulse, L. C. Johnson, N. R. Sauthoff, S. Sesnic, K. M. Young, M. Tavernier, et al., Phys. Rev. A **32**, 3011 (1985), URL http://link.aps.org/doi/10.1103/PhysRevA.32.3011.

[41] H. Hsuan, M. Bitter, K. W. Hills, S. von Goeler, B. Grek, D. Johnson, L. C. Johnson, S. Sesnic, C. P. Bhalla, K. R. Karim, et al., Phys. Rev. A **35**, 4280 (1987), URL http://journals.aps.org/pra/abstract/10.1103/PhysRevA.35.4280.

[42] W. M. Neupert, Solar Phys. **18**, 474 (1971), URL http://link.springer.com/article/10.1007%2FBF00149069?LI=true.

[43] K. Kubiçek, J. Braun, H. Bruhns, J. R. C. López-Urrutia, P. H. Mokler, and J. Ullrich, Rev. Sci. Instrum. **83**, 013102 (2012), URL http://link.aip.org/link/?RSI/83/013102/1http://dx.doi.org/10.1063/1.3662412.

[44] D. B. Thorn, M. F. Gu, G. V. Brown, P. Beiersdorfer, F. S. Porter, C. A. Kilbourne, and R. L. Kelley, Phys. Rev. Lett. **103**, 163001 (2009), URL http://link.aps.org/doi/10.1103/PhysRevLett.103.163001.

[45] T. F. R. Group, F. Bombarda, F. Bely-Dubau, P. Faucher, M. Cornille, J. Dubau, and M. Loulergue, Phys. Rev. A **32**, 2374 (1985), URL http://link.aps.org/doi/10.1103/PhysRevA.32.2374.

[46] J. E. Rice, M. L. Reinke, J. M. A. Ashbourn, C. Gao, M. Bitter, L. Delgado-Aparicio, K. Hill, N. T. Howard, J. W. Hughes, and U. I. Safronova, J. Phys. B: At. Mol. Opt. Phys. **48**, 144013 (2015), URL http://stacks.iop.org/0953-4075/48/i=14/a=144013.

[47] T. F. R. Group, M. Cornille, J. Dubau, and M. Loulergue, Phys. Rev. A **32**, 3000 (1985), URL https://link.aps.org/doi/10.1103/PhysRevA.32.3000.

[48] J. E. Rice, M. A. Graf, J. L. Terry, E. S. Marmar, K. Giesing, and F. Bombarda, J. Phys. B: At. Mol. Opt. Phys. **28**, 893 (1995), URL http://iopscience.iop.org/article/10.1088/0953-4075/28/5/021.

[49] J. E. Rice, M. L. Reinke, J. M. A. Ashbourn, C. Gao, M. M. Victora, M. A. Chilenski, L. Delgado-Aparicio, N. T. Howard, A. E. Hubbard, J. W. Hughes, et al., J. Phys. B: At. Mol. Opt. Phys. **47**, 075701 (2014), URL http://stacks.iop.org/0953-4075/47/i=7/a=

075701.

[50] P. Beiersdorfer, M. H. Chen, R. E. Marrs, M. B. Schneider, and R. S. Walling, Phys. Rev. A **44**, 396 (1991), URL http://link.aps.org/abstract/PRA/v44/p396.

[51] P. Beiersdorfer, T. Phillips, V. L. Jacobs, K. W. Hill, M. Bitter, S. von Goeler, and S. M. Kahn, The Astrophysical Journal **409**, 846 (1993), URL http://adsabs.harvard.edu/abs/1993ApJ...409..846B.

[52] S. Schlesser, S. Boucard, D. S. Covita, J. M. F. dos Santos, H. Fuhrmann, D. Gotta, A. Gruber, M. Hennebach, A. Hirtl, P. Indelicato, et al., Phys. Rev. A **88**, 022503 (2013), URL http://link.aps.org/doi/10.1103/PhysRevA.88.022503.

[53] C. T. Chantler and J. A. Kimpton, Can. J. Phys. **87**, 763 (2009).

[54] A. N. Artemyev, V. M. Shabaev, V. A. Yerokhin, G. Plunien, and G. Soff, Phys. Rev. A **71**, 062104 (2005), URL http://link.aps.org/abstract/PRA/v71/e062104.

[55] G. Plunien, B. Müller, W. Greiner, and G. Soff, Phys. Rev. A **43**, 5853 (1991), URL http://link.aps.org/doi/10.1103/PhysRevA.43.5853.

[56] G. Plunien and G. Soff, Phys. Rev. A **51**, 1119 (1995), URL http://journals.aps.org/pra/abstract/10.1103/PhysRevA.51.1119.

[57] G. Plunien and G. Soff, Phys. Rev. A **53**, 4614 (1996).

[58] T. Beier, P. J. Mohr, H. Persson, and G. Soff, Phys. Rev. A **58**, 954 (1998).

[59] K. S. Eikema, W. Ubachs, W. Vassen, and W. Hogervorst, Phys. Rev. Lett. **76**, 1216 (1996).

[60] K. S. Eikema, W. Ubachs, W. Vassen, and W. Hogervorst, Phys. Rev. A **55**, 1866 (1997).

[61] D. Z. Kandula, C. Gohle, T. J. Pinkert, W. Ubachs, and K. S. E. Eikema, Phys. Rev. A **84**, 062512 (2011), pRA, URL http://link.aps.org/doi/10.1103/PhysRevA.84.062512.

[62] K. Pachucki, J. Phys. B: At. Mol. Opt. Phys. **31**, 2489 (1998), URL http://stacks.iop.org/0953-4075/31/i=11/a=012.

[63] K. Pachucki, J. Phys. B: At. Mol. Opt. Phys. **31**, 3547 (1998), URL http://stacks.iop.org/0953-4075/31/i=16/a=008.

[64] K. Pachucki, Phys. Rev. A **74**, 022512 (2006), URL https://link.aps.org/doi/10.1103/PhysRevA.74.022512.

[65] K. Pachucki, Phys. Rev. A **74**, 062510 (2006), URL https://link.aps.org/doi/10.1103/PhysRevA.74.062510.

[66] V. A. Yerokhin and K. Pachucki, Phys. Rev. A **81**, 022507 (2010), URL http://link.aps.

org/doi/10.1103/PhysRevA.81.022507.

[67] I. Angeli and K. P. Marinova, At. Data Nucl. Data Tables **99**, 69 (2013), URL http://www.sciencedirect.com/science/article/pii/S0092640X12000265.

[68] E. Bulbul, M. Markevitch, A. Foster, R. K. Smith, M. Loewenstein, and W. R. Scott, The Astrophysical Journal **789**, 13 (2014), URL http://stacks.iop.org/0004-637X/789/i=1/a=13.

[69] A. Boyarsky, O. Ruchayskiy, D. Iakubovskyi, and J. Franse, Phys. Rev. Lett. **113**, 251301 (2014), URL http://link.aps.org/doi/10.1103/PhysRevLett.113.251301.

[70] C. Shah, S. Dobrodey, S. Bernitt, R. Steinbrgge, R. Crespo Lpez-Urrutia, J., L. Gu, and J. Kaastra, The Astrophysical Journal **833**, 52 (2016), URL http://stacks.iop.org/0004-637X/833/i=1/a=52.

[71] V. M. Shabaev, I. I. Tupitsyn, and V. A. Yerokhin, Phys. Rev. A **88**, 012513 (2013), URL http://link.aps.org/doi/10.1103/PhysRevA.88.012513.

[72] R. D. Deslattes, Rev. Sci. Instrum. **38**, 815 (1967).

[73] P. Amaro, C. I. Szabo, S. Schlesser, A. Gumberidze, E. G. Kessler, A. Henins, E. O. Le Bigot, M. Trassinelli, J. M. Isac, P. Travers, et al., Radiat. Phys. and Chem. **98**, 132 (2014).

[74] A. Gumberidze, M. Trassinelli, N. Adrouche, C. I. Szabo, P. Indelicato, F. Haranger, J. M. Isac, E. Lamour, E. O. Le Bigot, J. Merot, et al., Rev. Sci. Instrum. **81**, 033303 (2010).

[75] M. Guerra, P. Amaro, C. I. Szabo, A. Gumberidze, P. Indelicato, and J. P. Santos, J. Phys. B: At. Mol. Opt. Phys. **46**, 065701 (2013), URL http://stacks.iop.org/0953-4075/46/i=6/a=065701.

[76] H. Fujimoto, A. Waseda, and X. W. Zhang, Metrologia **48**, S55 (2011).

[77] P. Mohr, B. Taylor, and D. Newell, Rev. Mod. Phys. **84**, 1527 (2012).

[78] E. G. Kessler, C. I. Szabo, J. P. Cline, A. Henins, L. T. Hudson, M. H. Mendenhall, and M. D. Vaudin, J. Res. NIST **To be published.** (2017).

[79] M. Sanchez del Rio and J. Dejus, in SPIE proceedings (1998), p. 3448.

[80] W. H. Zachariasen, Theory of X-ray diffraction in crystals (Dover Publications, New York, 1967).

[81] S. Stepanov, URL http://sergey.gmca.aps.anl.gov/x0h.html.

[82] O. M. Lugovskaya and S. A. Stepanov, Soviet physics. Crystallography **36**, 478 (1991).

[83] W. H. Press, B. P. Flannery, S. A. Teukolsky, and W. T. Vetterling,

Numerical Recipes 3rd Edition: The Art of Scientific Computing (Cambridge University Press, Cambridge, 2007).

[84] R. Brun and F. Rademakers, Nucl. Instr. Methods A **389**, 81 (1997), URL http://www.sciencedirect.com/science/article/pii/S016890029700048X.

[85] I. Antcheva, M. Ballintijn, B. Bellenot, M. Biskup, R. Brun, N. Buncic, P. Canal, D. Casadei, O. Couet, V. Fine, et al., Comp. Phys. Commun. **180**, 2499 (2009), URL http://www.sciencedirect.com/science/article/pii/S0010465509002550.

[86] I. Antcheva, M. Ballintijn, B. Bellenot, M. Biskup, R. Brun, N. Buncic, P. Canal, D. Casadei, O. Couet, V. Fine, et al., Comp. Phys. Commun. **182**, 1384 (2011), URL http://www.sciencedirect.com/science/article/pii/S0010465511000701.

[87] Wolfram Research, Mathematica 11.0 (2016).

[88] V. A. Yerokhin, A. Surzhykov, and S. Fritzsche, Phys. Rev. A **90**, 022509 (2014), URL http://link.aps.org/doi/10.1103/PhysRevA.90.022509.

[89] V. A. Yerokhin, A. Surzhykov, and S. Fritzsche, Phys. Scr. **90**, 054003 (2015), URL http://stacks.iop.org/1402-4896/90/i=5/a=054003.

[90] U. I. Safronova and A. M. Urnov, J. Phys. B: At. Mol. Opt. Phys. **12**, 3171 (1979), URL http://stacks.iop.org/0022-3700/12/3171.

[91] U. I. Safronova and T. G. Lisina, At. Data Nucl. Data Tables **24**, 49 (1979), URL http://www.sciencedirect.com/science/article/B6WBB-4DBJ1Y8-8N/2/651d76743f03f845389d5c8312723a70.

[92] M. H. Chen, Phys. Rev. A **31**, 1449 (1985), URL http://dx.doi.org/10.1103/PhysRevA.31.1449.

[93] M. H. Chen and B. Crasemann, Can. J. Phys. **37**, 419 (1987), URL http://www.sciencedirect.com/science/article/B6WBB-4DBJ6GP-4X/2/9176119bceb9511d4295a42c95064c5a.

[94] J. P. Desclaux, Comp. Phys. Commun. **9**, 31 (1975).

[95] P. Indelicato and J. P. Desclaux, Phys. Rev. A **42**, 5139 (1990), URL http://journals.aps.org/pra/abstract/10.1103/PhysRevA.42.5139.

[96] P. Indelicato, O. Gorceix, and J. P. Desclaux, J. Phys. B: At. Mol. Opt. Phys. **20**, 651 (1987), URL http://dx.doi.org/10.1088/0022-3700/20/4/007.

[97] P. Indelicato and J. Desclaux, Mcdfgme, a multiconfiguration dirac fock and general matrix elements progra

http://kroll.lkb.upmc.fr/mcdf (2005).

[98] I. P. Grant and H. M. Quiney, Adv. At. Mol. Phys. **23**, 37 (1988).

[99] P. Indelicato, Phys. Rev. A **51**, 1132 (1995).

[100] V. M. Shabaev, Theoretical and Mathematical Physics **63**, 588 (1985).

[101] V. M. Shabaev and A. N. Artemyev, J. Phys. B: At. Mol. Opt. Phys. **27**, 1307 (1994).

[102] V. M. Shabaev, Phys. Rev. A **57**, 59 (1998).

[103] J. M. Sampaio, F. Parente, C. Naz, M. Godefroid, P. Indelicato, and J. P. Marques, Physica Scripta **2013**, 014015 (2013), URL http://stacks.iop.org/1402-4896/2013/i=T156/a=014015.

[104] J. P. Santos, J. P. Marques, F. Parente, E. Lindroth, P. Indelicato, and J. P. Desclaux, J. Phys. B: At. Mol. Phys. **32**, 2089 (1999).

[105] J. P. Santos, G. C. Rodrigues, J. P. Marques, F. Parente, J. P. Desclaux, and P. Indelicato, Eur. Phys. J. D **37**, 201 (2006), URL http://www.springerlink.com/openurl.asp?genre=article&id=doi:10.1140/epjd/e2006-00002-x.

[106] M. C. Martins, J. P. Marques, A. M. Costa, J. P. Santos, F. Parente, S. Schlesser, E. O. Le Bigot, and P. Indelicato, Phys. Rev. A **80**, 032501 (2009).

[107] G. Audi, A. H. Wapstra, and C. Thibault, Nucl. Phys. A **729**, 337 (2003).

[108] I. Angeli, Can. J. Phys. **87**, 185 (2004).

[109] P. J. Mohr and Y.-K. Kim, Phys. Rev. A **45**, 2727 (1992), URL http://link.aps.org/doi/10.1103/PhysRevA.45.2727.

[110] P. J. Mohr, Phys. Rev. A **46**, 4421 (1992).

[111] E.-O. Le Bigot, P. Indelicato, and P. J. Mohr, Phys. Rev. A **64**, 052508 (14) (2001).

[112] P. Indelicato and P. J. Mohr, Phys. Rev. A **46**, 172 (1992).

[113] P. J. Mohr and G. Soff, Phys. Rev. Lett. **70**, 158 (1993).

[114] P. Indelicato and E. Lindroth, Phys. Rev. A **46**, 2426 (1992).

[115] P. Indelicato, S. Boucard, and E. Lindroth, Eur. Phys. J. D **3**, 29 (1998).

[116] P. Indelicato and P. Mohr, Hyp. Int. **114**, 147 (1998).

[117] V. M. Shabaev, I. I. Tupitsyn, and V. A. Yerokhin, Comp. Phys. Commun. **189**, 175 (2015), URL http://www.sciencedirect.com/science/article/pii/S0010465514004081.

[118] P. Indelicato, F. Parente, and R. Marrus, Phys. Rev. A **40**, 3505 (1989).

[119] P.-O. Löwdin, Phys. Rev. **97**, 1474 (1955).

[120] P. Indelicato, Hyperfine Interaction **108**, 39 (1997).

[121] C. Froese Fischer, The Hartree-Fock Method for Atoms (Wiley, New York, 1977).

[122] O. Gorceix, P. Indelicato, and J. P. Desclaux, J. Phys. B: At. Mol. Opt. Phys. **20**, 639 (1987), URL http://dx.doi.org/10.1088/0022-3700/20/4/006.

[123] P. Indelicato, Phys. Rev. Lett. **77**, 3323 (1996), URL http://link.aps.org/doi/10.1103/PhysRevLett.77.3323.

[124] G. Howat, T. Åberg, and O. Goscinski, J. Phys. B: At. Mol. Opt. Phys. **11**, 1575 (1978), URL http://iopscience.iop.org/article/10.1088/0022-3700/11/9/011/meta.

[125] A. M. Costa, M. C. Martins, F. Parente, J. P. Santos, and P. Indelicato, Can. J. Phys. **79**, 223 (2001), URL http://www.idealibrary.com/links/doi/10.1006/adnd.2001.0869.

[126] L. Natarajan, J. Phys. B: At. Mol. Opt. Phys. **36**, 105 (2003), URL http://stacks.iop.org/0953-4075/36/i=1/a=308.

[127] M. F. Gu, Can. J. Phys. **86**, 675 (2008), URL http://www.nrcresearchpress.com/doi/abs/10.1139/p07-197.

[128] G. W. F. Drake, Phys. Rev. A **19**, 1387 (1979), URL http://link.aps.org/doi/10.1103/PhysRevA.19.1387.

[129] W. R. Johnson, D. R. Plante, and J. Sapirstein, in Advances in Atomic, Molecular and Optical Physics, edited by B. Bederson and H. Walters (Addison-Wesley, New York, 1995), vol. 35, pp. 255–329.

[130] A. Derevianko, I. M. Savukov, W. R. Johnson, and D. R. Plante, Phys. Rev. A **58**, 4453 (1998).

[131] P. Indelicato, V. M. Shabaev, and A. V. Volotka, Phys. Rev. A **69**, 062506 (2004), URL http://link.aps.org/abstract/PRA/v69/e062506.

[132] C. I. Szabo, P. Amaro, M. Guerra, S. Schlesser, A. Gumberidze, J. P. Santos, and P. Indelicato, in CAARI (AIP, Fort Worth, Texas, 2013), vol. 1525 of AIP Conference Proceedings, pp. 68–72.

[133] C. I. Szabo, P. Amaro, M. Guerra, J. P. Santos, A. Gumberidze, J. Attard, and P. Indelicato, Phys. Scr. **2013**, 014077 (2013), URL http://stacks.iop.org/1402-4896/2013/i=T156/a=014077.

[134] D. R. Plante, W. R. Johnson, and J. Sapirstein, Phys. Rev. A **49**, 3519 (1994).

[135] K. T. Cheng, M. H. Chen, W. R. Johnson, and J. Sapirstein, Phys. Rev. A **50**, 247 (1994).

[136] G. W. Drake, Can. J. Phys. **66**, 586 (1988).

[137] U. I. Safronova, Phys. Scr. **23**, 241 (1981).

[138] W. R. Johnson and J. Sapirstein, Phys. Rev. A **46**, R2197 (1992).

[139] A. H. Gabriel, Mon. Not. R. Astron. Soc. **160**, 99 (1972).

[140] L. Engstrom and U. Litzen, J. Phys. B: At. Mol. Opt. Phys. **28**, 2565 (1995), URL http://stacks.iop.org/0953-4075/28/i=13/a=010.

[141] L. Schleinkofer, F. Bell, H. D. Betz, G. Trolman, and J. Rothermel, Physica Scripta **25**, 917 (1982), URL http://dx.doi.org/10.1088/0031-8949/25/6B/004.

[142] H. D. Dohmann, D. Liesen, and H. Pfeng, Zeitschrift fr Physik A Hadrons and Nuclei **285**, 171 (1978), URL http://dx.doi.org/10.1007/BF01408743.

[143] P. Beiersdorfer, M. Bitter, S. von Goeler, and K. W. Will, Phys. Rev. A **40**, 150 (1989), URL http://journals.aps.org/pra/abstract/10.1103/PhysRevA.40.150.

[144] C. T. Chantler, D. Paterson, L. T. Hudson, F. G. Serpa, J. D. Gillaspy, and E. Takacs, Phys. Rev. A **62**, 042501/1 (2000), URL http://publish.aps.org/abstract/PRA/v62/p042501.

[145] J. P. Briand, M. Tavernier, R. Marrus, and J. P. Desclaux, Phys. Rev. A **29**, 3143 (1984), URL http://link.aps.org/doi/10.1103/PhysRevA.29.3143.

[146] S. MacLaren, P. Beiersdorfer, D. A. Vogel, D. Knapp, R. E. Marrs, K. Wong, and R. Zasadzinski, Phys. Rev. A **45**, 329 (1992), URL http://link.aps.org/doi/10.1103/PhysRevA.45.329.

[147] P. Indelicato, M. Tavernier, J. P. Briand, and D. Liesen, Zeitschrift fr Physik D **2**, 249 (1986).

[148] K. Widmann, P. Beiersdorfer, V. Decaux, and M. Bitter, Phys. Rev. A **53**, 2200 (1996), URL http://link.aps.org/doi/10.1103/PhysRevA.53.2200.

[149] J. P. Briand, P. Indelicato, A. Simionovici, V. San Vicente, D. Liesen, and D. Dietrich, Europhysics Letters **9**, 225 (1989), URL http://iopscience.iop.org/0295-5075/9/3/007.

[150] J. P. Briand, P. Chevallier, P. Indelicato, D. Dietrich, and K. Ziock, Phys. Rev. Lett. **65**, 2761 (1990).

[151] V. Decaux, P. Beiersdorfer, S. M. Kahn, and V. L. Jacobs, The Astrophysical Journal **482**, 1076 (1997).

[152] D. B. Thorn, G. V. Brown, J. H. T. Clementson, H. Chen, M. Chen, P. Beiersdorfer, K. R. Boyce, C. A. Kilbourne, F. S. Porter, and R. L. Kelley, Can. J. Phys. **86**, 241 (2008).

[153] R. Steinbrgge, S. Bernitt, S. W. Epp, J. K. Rudolph, C. Beilmann, H. Bekker, S. Eberle,

A. Müller, O. O. Versolato, H. C. Wille, et al., Phys. Rev. A **91**, 032502 (2015), URL http://link.aps.org/doi/10.1103/PhysRevA.91.032502.

[154] U. I. Safronova and A. S. Shlyaptseva, Physica Scripta **54**, 254 (1996), URL http://stacks.iop.org/1402-4896/54/i=3/a=005.

[155] V. A. Boiko, A. Y. Chugunov, T. G. Ivanova, A. Y. Faenov, I. V. Holin, S. A. Pikuz, A. M. Urnov, L. A. Vainshtein, and U. I. Safronova, Monthly Notices of the Royal Astronomical Society **185**, 305 (1978), URL http://dx.doi.org/10.1093/mnras/185.2.305.

[156] S. Shuqiang, P. Feng, and J. Gang, J. Phys. B: At. Mol. Opt. Phys. **39**, 2087 (2006), URL http://stacks.iop.org/0953-4075/39/i=8/a=023.

TABLE VI: Comparison of our He-like argon experimental $1s2p\,^1P_1 \rightarrow 1s^2\,^1S_0$ transition energy with previous experimental and theoretical values. All energies are given in eV, and estimated uncertainties are shown in parentheses.

Energy	Reference	Exp. method
	Experiment	
3139.5927 (50)(57)(76)	This Work (stat.)(syst.)(tot.)	ECRIS
3139.567 (11)	Schlesser *et al.* (2013) [52]	ECRIS
3139.581 (5)	Kubiček *et al.* (2012) [43]	EBIT
3139.583 (63)	Bruhns *et al.* (2007) [1]	EBIT
3139.552 (37)	Deslattes *et al.* (1984) [39]	Recoil ions
3139.60 (25)	Briand *et al.* (1983) [35]	Beam-foil
3140.1 (7)	Dohmann *et al.* (1979) [34]	Beam-foil
3138.9 (9)	Neupert *et al.* (1971) [42]	Solar emission
	Theory	
3139.544 (5) (40)	This work using Welton model (correlation) (Welton)	
3139.584 (6)	This work using model operators [71, 117]	
3139.5821 (4)	Artemyev *et al.* (2005) [54]	
3139.582	Plante *et al.* (1994) [134]	
3139.617	Cheng *et al.* (1994) [135]	
3139.576	Drake (1988) [136]	
3139.649	Indelicato *et al.* (1987) [96]	
3139.56	Safronova (1981) [137]	
3140.15	Johnson *et al.* (1976) [138]	
3140.46	Gabriel (1972) [139]	

TABLE VII: Summary of all measured in $n = 2 \rightarrow n = 1$ transition energies in He-like ions $7 \leq Z \leq 20$. The theoretical values are from Ref. [54], which are available for $Z \geq 12$. The experimental values are either reference-free measurements (RF) or measurements calibrated against standard reference x-ray transitions, or hydrogen-like transitions (SR).

	$1s2p\,^1P_1 \rightarrow 1s^2\,^1S_0$ (w)			$1s2p\,^3P_2 \rightarrow 1s^2\,^1S_0$ (x)			$1s2p\,^3P_1 \rightarrow 1s^2\,^1S_0$ (y)			$1s2s\,^3S_1 \rightarrow 1s^2\,^1S_0$ (z)				
Z	Exp. (eV)	Err.	Theory	Exp. (eV)	Err.	Theory	Exp. (eV)	Err.	Theory	Exp. (eV)	Err.	Theory	Method	Ref.
7	430.6870	0.0030											SR	[140]
8	573.9491	0.0106											SR	[140]
11	1126.7194	0.3072											SR	[33]
12	1352.3287	0.0148	1352.2483			1343.5417			1343.0988			1331.1118	SR	[33]
13	1598.4555	0.3091	1598.2914			1588.7611			1588.1254			1574.9799	SR	[33]
14	1864.7605	0.4207	1865.0014			1854.6679			1853.7804			1839.4495	SR	[33]
15	2152.8398	0.5607	2152.431			2141.3188			2140.1082			2124.5619	SR	[33]
16	2461.2736	0.4886	2460.6292			2448.7628			2447.1439			2430.3512	SR	[33]
16	2460.6300	0.0214	2460.6292			2448.7628			2447.1439			2430.3512	RF	[7]
16	2460.6700	0.0900	2460.6292			2448.7628	2447.05	0.11	2447.1439			2430.3512	SR	[141]
18			3139.5821			3126.2896			3123.5344	3104.1605	0.0077	3104.1483	RF	[2]
18			3139.5821	3128	2	3126.2896			3123.5344			3104.1483	RS	[142]
18	3139.5927	0.0076	3139.5821			3126.2896			3123.5344			3104.1483	RF	this work
18	3139.5810	0.0092	3139.5821			3126.2896			3123.5344			3104.1483	RF	[7]
18	3139.552	0.037	3139.5821	3126.283	0.036	3126.2896	3123.521	0.036	3123.5344			3104.1483	SR	[39]
18	3139.57	0.25	3139.5821	3126.37	0.40	3126.2896	3123.57	0.24	3123.5344			3104.1483	SR	[35]
19	3510.58	0.12	3510.4616			3496.4937			3492.9736			3472.2417	SR	[143]
20	3902.19	0.12	3902.3777	3887.63	0.12	3887.7607	3883.24	0.12	3883.3169	3861.11	0.12	3861.2059	SR	[49]

TABLE VIII: Summary of all measured in $n = 2 \rightarrow n = 1$ transition energies in He-like ions $21 \leq Z \leq 92$. The theoretical values are from Ref. [54]. The experimental values are either reference-free measurements (RF) or measurements calibrated against standard reference x-ray transitions, or hydrogen-like transitions (SR).

	$1s2p\,^1P_1 \rightarrow 1s^2\,^1S_0$ (w)			$1s2p\,^3P_2 \rightarrow 1s^2\,^1S_0$ (x)			$1s2p\,^3P_1 \rightarrow 1s^2\,^1S_0$ (y)			$1s2s\,^3S_1 \rightarrow 1s^2\,^1S_0$ (z)				
Z	Exp. (eV)	Err.	Theory	Exp. (eV)	Err.	Theory	Exp. (eV)	Err.	Theory	Exp. (eV)	Err.	Theory	Method	Ref.
21	4315.54	0.15	4315.4124			4300.1720			4294.6220			4271.0997	SR	[143]
21	4315.35	0.15	4315.4124	4300.23	0.15	4300.1720	4294.57	0.15	4294.6220	4271.19	0.15	4271.0997	SR	[48]
22	4749.73	0.17	4749.6441			4733.8008			4726.9373			4701.9746	SR	[143]
22	4749.852	0.072	4749.6441	4733.83	0.13	4733.8008	4727.07	0.10	4726.9373	4702.078	0.072	4701.9746	SR	[6]
23	5205.26	0.21	5205.1653			5188.7378			5180.3264			5153.8962	SR	[143]
23	5205.10	0.14	5205.1653	5189.120	0.210	5188.7378	5180.22	0.17	5180.3264	5153.82	0.14	5153.8962	SR	[144]
24	5682.32	0.40	5682.0684			5665.0715			5654.8491			5626.9276	SR	[143]
26	6700.73	0.20	6700.4347			6682.3339			6667.5786			6636.6126	SR	[143]
26	6700.441	0.049	6700.4347			6682.3339			6667.5786			6636.6126	SR	[7]
26	6700.90	0.25	6700.4347	6682.50	0.25	6682.3339	6667.50	0.25	6667.5786			6636.6126	RF	[145]
26	6700.549	0.070	6700.4347			6682.3339	6667.671	0.069	6667.5786			6636.6126	SR	[4]
29	8390.82	0.15	8391.0349	8371.17	0.15	8371.3181	8346.99	0.15	8346.9929	8310.83	0.15	8311.3467	RF	[8]
32	10280.70	0.22	10280.2175	10259.52	0.37	10258.8739	10221.79	0.35	10220.7996	10181.33	0.52	10180.3868	SR	[146]
36	13115.45	0.30	13114.4705			13090.8657	13026.8	3.0	13026.1165			12979.2656	SR	[147]
36	13114.68	0.36	13114.4705	13091.17	0.37	13090.8657	13026.29	0.36	13026.1165	12979.63	0.41	12979.2656	SR	[148]
36	13114.47	0.14	13114.4705			13090.8657	13026.15	0.14	13026.1165			12979.2656	SR	[9]
54	30629.1	3.5	30630.0512			30594.3635	30209.6	3.5	30206.2652			30129.1420	RF	[149]
54	30631.2	1.2	30630.0512	30594.5	1.7	30594.3635	30207.1	1.4	30206.2652	30128.6	1.3	30129.1420	SR	[44]
92	100626	35	100610.89			100537.18			96169.63			96027.15	SR	[150]

TABLE IX: Summary of all measured in $n = 2 \to n = 1$ transition energies in He-like ions $Z \geq 7$. The theoretical values are from Ref. [54], which are available for $Z \geq 12$. The experimental values are calibrated against one of the He-like transition (x, y, z or w), noted "Ref.". The energies have been re-evaluated using Ref. [54] for the reference transition energy.

	$1s2p\,^1P_1 \to 1s^2\,^1S_0$ (w)			$1s2p\,^3P_2 \to 1s^2\,^1S_0$ (x)			$1s2p\,^3P_1 \to 1s^2\,^1S_0$ (y)			$1s2s\,^3S_1 \to 1s^2\,^1S_0$ (z)			
Z	Exp. (eV)	Err.	Theory	Exp. (eV)	Err.	Theory	Exp. (eV)	Err.	Theory	Exp. (eV)	Err.	Theory	Ref.
16			2460.6292	2448.739	0.020	2448.7628	2447.150	0.009	2447.1439	Ref.		2430.3512	[52]
18	3139.567	0.011	3139.5821	3126.291	0.011	3126.2896	3123.489	0.012	3123.5344	Ref.		3104.1483	[52]
18	Ref.		3139.5821	3126.440	0.079	3126.2896	3123.604	0.079	3123.5344	3104.21	0.16	3104.1483	[45]
21	Ref.		4315.4124	4300.00	0.30	4300.1720	4294.49	0.30	4294.6220	4271.99	0.29	4271.0997	[47]
22	Ref.		4749.6441	4733.86	0.18	4733.8008	4726.82	0.18	4726.9373	4701.89	0.18	4701.9746	[40]
23	Ref.		5205.1653	5188.18	0.43	5188.7378	5179.51	0.43	5180.3264	5153.24	0.43	5153.8962	[47]
24	Ref.		5682.0684	5664.67	0.52	5665.0715	5654.60	0.52	5654.8491	5626.63	0.51	5626.9276	[47]
25	Ref.		6180.4573	6163.25	0.61	6162.9043	6150.11	0.61	6150.5777	6120.66	0.60	6121.1432	[47]
28	Ref.		7805.6053	7786.96	0.49	7786.4246			7765.7048			7731.6307	[41]

TABLE X: Measured and computed natural line width values for the $1s2s^22p\,^1P_1 \rightarrow 1s^22s^2\,^1S_0$ transition in Be-like Ar. All values are given in meV, and estimated uncertainties are shown in parentheses.

Transition	Experiment	Theory	Reference
$1s2s^22p\,^1P_1 \rightarrow 1s^22s^2\,^1S_0$	145 (18)	126.9	MCDF (this work)
		121.4	FAC (this work)
		106.1	Safronova *et al.* (1979) [91]
		146.8	Chen (1985) [92]
		150.9	Costa *et al.* (2001) [125]

TABLE XI: Comparison between experimental and theoretical Be-like argon $1s2s^22p\,^1P_1 \rightarrow 1s^22s^2\,^1S_0$ transition energies. All energies are given in eV, and estimated uncertainties are shown in parentheses.

Transition energy	Reference
Experiment	
3091.7771(61)(50)(83)	This work (stat.)(syst.)(tot.)
3091.776(3)	Schlesser *et al.* (2013) [52]
Theory	
3091.7729(77)	This work using model operators [71, 117] (see Table II)
3091.748(41)	This work using Welton model (see Table II)
3091.11	This work using FAC [127]
3091.749(34)	Yerokhin *et al.* (2015) [89]
3088.958	Natarajan (2003) [126]
3091.95	Costa *et al.* (2001) [125]
3092.157	Safronova and Shlyaptseva (1996) [154]
3090.64	Chen and Crasemann (1987) [93]
3090.66	Chen (1985) [92]
3092.18	Safronova and Lisina (1979) [91]
3092.18	Boiko *et al.* (1978) [155]